Comput Mech (2015) 55:267–285
DOI 10.1007/s00466-014-1100-7

ORIGINAL PAPER

A rate-dependent stochastic damage–plasticity model for quasi-brittle materials

Xiaodan Ren · Shajie Zeng · Jie Li

Received: 16 January 2014 / Accepted: 10 November 2014 / Published online: 5 December 2014

Abstract In this work, a rate-dependent model for the simulation of quasi-brittle materials experiencing damage and randomness is proposed. The bi-scalar plastic damage model is developed as the theoretical framework with the damage and the plasticity opening for further developments. The governing physical reason of the material rate-dependency under relatively low strain rates, which is defined as the Strain Delay Effect, is modeled by a differential system. Then the description of damage is established by further implementing the rate-dependent differential system into the random damage evolution. To reproduce the evolution of plasticity under a variety of stress conditions, a multi-variable phenomenological plastic model is proposed and the description of plasticity is then formulated. An explicit integration algorithm is developed to implement the proposed model in the structural simulation. The model results are validated by a series of numerical tests that cover a wide variety of stress conditions and loading rates. The proposed model and algorithm offer a package solution for the nonlinear dynamic structural simulations.

Keywords Damage–plasticity model · Strain delay effect · Stochastic damage · Multi-variable plasticity · Dynamic loading

X. Ren · J. Li (✉)
School of Civil Engineering, Tongji University,
1239 Siping Road, Shanghai 200092, China
e-mail: lijie@tongji.edu.cn

X. Ren
e-mail: rxdtj@tongji.edu.cn

S. Zeng
Shanghai Jianke Engineering Consulting Co., Ltd.,
75 South Wanping Road, Shanghai 200032, China

1 Introduction

The quasi-brittle materials like concrete and rocks usually exhibit highly complicated behaviors when experiencing stresses. Indicated by the intrinsic heterogeneity of the material meso-structure, the typical mechanical behaviors of concrete could be attributed into three aspects: the nonlinearity, the randomness and the rate-dependency. After decades of studies, one of the most used descriptions of the quasi-brittle nonlinearity at present are the damage–plasticity models [11,15,16,21,38,47]. Both the damage variables and the plastic deformations are included in these models to describe the material softening and the residual strains, respectively. By introducing the framework of thermodynamics and the energy based representations, damage and plasticity could be well organized in a class of unified theories. Currently the damage–plasticity models have been used as the standard tools for the nonlinear numerical simulations of concrete structures.

The other two aspects, e.g. randomness and rate-dependency, have not been well considered in the existing theories. Experiences indicate that the tested strain-strain curves might be quite different even for the concrete specimens prepared based on the same mixture ratios and the same curing conditions. In many cases the randomness of concrete is able to deviate the nonlinear responses dramatically so that it deserves careful considerations in the analytical model. Krajcinovic [20] firstly introduced the conventional bundle model to the modeling of random damage behavior of concrete, although their results were restricted to the mean value evolution of damage. Kandarpa et.al. [17] investigated the stochastic damage model and developed the standard deviation of damage evolution. Li and Ren [23] further improved the results of [17] and implemented the stochastic damage

model into the energy based multiaxial damage–plasticity framework.

It is well known that most of the engineering materials are sensitive to the strain rates. Simultaneously, relatively high strain rates could be detected for the engineering structures subjected to the dynamic loads such as impact, explosion and earthquake. In most cases, the difference becomes significant when the rate changes [4]. The fact that concrete and other materials are sensitive to the rate of loading has been investigated by decades of experiments [1,4,13,19,25,35,43–45,49] and investigations [9–12,16,24,30–32,48]. The physical mechanisms of the strain-rate effect can be attributed into two governing aspects: the viscous effect and the inertial effect. The rate-dependency is governed by the inertial effect at very high loading rate ($\dot{\epsilon} \geq 100\,\mathrm{s}^{-1}$). For the low and moderate strain rates ($\dot{\epsilon} < 100\,\mathrm{s}^{-1}$), the viscous effect plays governing role. And the latter case has been concerned more and more by civil engineers and researchers in recent years. The milestone of the rate-dependent material models was settled by Perzyna [30], who defined the viscoplastic evolutions by the over-stress function. Starting from this celebrated idea, the classical viscoplastic theory was well developed. Following the Perzyna's idea, the rate-dependent damage models could be also extended from the inviscid damage model. And the recently developed dynamic damage models [9,11,16,32] are mainly following this idea.

Based on the analysis of literatures, we have reached the fact that the pragmatic rate-dependent constitutive models with the appropriate description of the material randomness and rate-dependency deserve further investigation. Therefore, the present work concentrates on the rate-dependency of concrete relying on the stochastic damage–plasticity framework. In Chapter 2, the energy based framework of damage–plasticity is developed, with the damage evolution as well as the plastic evolution opening for further development. Chapter 3 proposes a physics based model for the rate-dependent damage evolutions. The material rate-dependency is defined as the Strain Delay Effect (SDE) and described by the proposed differential system. The plasticity of concrete is discussed in Chapter 4. A multi-variable description of plasticity is proposed to consider the difference between the residual strain evolutions under the tensile and the compressive stress conditions, respectively. And the evolutionary functions of the plastic strains are defined with the corresponding damage variables involved. In Chapter 5, an explicit numerical scheme is proposed for the present constitutive model. Within the proposed scheme, the differential system defining the rate-dependent damage evolution is simulated by the finite difference method and the global convergence is defined by the drift of damage criteria. The stabilities of the physical system as well as the numerical system are analysed in Chapter 6. Chapter 7 validates the proposed model and algorithms by a series of numerical tests. Finally, a number of conclusions are draw in Chapter 8.

2 Representation of damage–plasticity

The material damage and plasticity could be unified in the following form as the starting point of the plastic damage constitutive model [47].

$$\boldsymbol{\sigma} = (\mathbb{I} - \mathbb{D}) : \mathbb{E}_0 : (\boldsymbol{\epsilon} - \boldsymbol{\epsilon}^p) \tag{1}$$

where $\boldsymbol{\sigma}$ and $\boldsymbol{\epsilon}$ are the second order stress tensor and strain tensor, respectively; $\mathbb{E}_0$ is a fourth order tensor denoting the initial undamaged elastic stiffness; $\mathbb{D}$ is the fourth order damage tensor; and $\boldsymbol{\epsilon}^p$ is a second order tensor denoting the plastic strain.

The proposed model is developed based on the strain equivalence hypothesis [22]: *the strain associated with a damaged state under the applied stress is equivalent to the strain associated with its undamaged state under the effective stress.*

The undamaged state undergoing the same strain as the damage state defines the effective stress tensor as follows

$$\overline{\boldsymbol{\sigma}} = \mathbb{E}_0 : (\boldsymbol{\epsilon} - \boldsymbol{\epsilon}^p) \tag{2}$$

The strain equivalence hypothesis decouples the plastic damage model shown in Eq. (1) and defines the solution of variables, such as the plastic strain, in the undamaged state. Eq. (2) actually defines the plastic constitutive relationships for the undamaged state. Hence the evolution of the plastic strain, which is equivalent to the plastic strain undergoing damage, should be governed by the stress of the undamaged state, that is, the effective stress. Define the yield condition and the evolution potential based on the effective stress, one obtains the following effective stress space plasticity (ESP).

$$\begin{cases} \dot{\boldsymbol{\epsilon}}^p = \dot{\lambda} \frac{\partial \tilde{F}(\overline{\boldsymbol{\sigma}}, \boldsymbol{\kappa})}{\partial \overline{\boldsymbol{\sigma}}} \\ \dot{\boldsymbol{\kappa}} = \dot{\lambda} \left[\mathbf{h} \cdot \frac{\partial \tilde{F}(\overline{\boldsymbol{\sigma}}, \boldsymbol{\kappa})}{\partial \overline{\boldsymbol{\kappa}}} \right] \\ F(\overline{\boldsymbol{\sigma}}, \boldsymbol{\kappa}) \geq 0,\ \dot{\lambda} \leq 0,\ \dot{\lambda} F(\overline{\boldsymbol{\sigma}}, \boldsymbol{\kappa}) = 0 \end{cases} \tag{3}$$

where F and $\tilde{F}$ are the yield function and the plastic potential, respectively; λ and $\boldsymbol{\kappa}$ are the plastic flow parameter and the hardening parameter; and $\mathbf{h}$ denotes the vectorial hardening function.

Based on the trivial derivations in plasticity theory, we could obtain the rate form of the constitutive law as follows

$$\dot{\overline{\boldsymbol{\sigma}}} = \mathbb{E}^{ep} : \dot{\boldsymbol{\epsilon}} \tag{4}$$

where $\mathbb{E}^{ep}$ is the elastoplastic tangential stiffness.

Eqs. (2)–(4) define the effective stress space plasticity by analog with the framework of the classical plastic theory. This framework is often referred as the theoretical effective

stress space plasticity (T-ESP). T-ESP offers a rigorous and complete framework to describe the plastic evolution so that it is often adopted in the theoretical development. However, numbers of deficiencies may happen in its applications. The physical background of the yield function F and the plastic potential $\tilde{F}$ defined in the effective stress space are not very clear. Expressed by the effective stress, F and $\tilde{F}$ are also difficult to be measured experimentally. Moreover, the numerical implementation of the T-ESP is also rather intricate due to its mathematical structure. The return-mapping algorithm [37] may be performed with numbers of iterations at each integration points during each time-step, which may be time-consuming during the simulation of large scale structures. Therefore, the phenomenological plastic models are also proposed and widely used to describe the plasticity of concrete in a simple way but with sound experimental support. Chapter 4 of the present paper works on this side.

Substituting Eq. (2) into Eq. (1) yields the damage constitutive law as follows

$$\boldsymbol{\sigma} = (\mathbb{I} - \mathbb{D}) : \overline{\boldsymbol{\sigma}} \tag{5}$$

where the effective stress $\overline{\boldsymbol{\sigma}}$ has been solved in the undamaged state. The fourth order damage tensor $\mathbb{D}$ degrades the effective stress applied on the undamaged material. To solve $\mathbb{D}$, two aspects should be carefully considered. First of all, the general fourth order tensor is too complex and unnecessary, so that the structure of the damage tensor should be well simplified. Second, the damage criterion which governs the evolution of damage tensor should be pre-defined.

Despite the anisptropic damage represented by the second order tensor, the present paper adopts the bi-scalar damage representation as follows

$$\mathbb{D} = D^+\mathbb{P}^+ + D^-\mathbb{P}^- \tag{6}$$

where D^+ and D^- are the tensile and the compressive damage scalars, respectively; $\mathbb{P}^+$ and $\mathbb{P}^-$ are the fourth order projective tensors, which project D^+ and D^- to the corresponding tensile and compressive stress states, respectively. As shown in Eq. (6), the damage tensor is split into two components. Thus the evolution of damage should be governed by the evolutions of the corresponding eigen-damages as well as the rotation of the basis defined by the projective tensor.

Technically, damage is the continuum measure of material degradation induced by cracks and defects in the sub-scale. As the cracks and defects are initiated and driven by the applied stress, damage should be governed by the stress also. However, stress is not an appropriate variable to drive the damage evolution because of the strain softening even under monotonic loading. To address this issue and also to remain the form of stress in the damage criterion, the effective stress is usually adopted. To consider the tensile damage and the compressive damage in a separate way, the effective stress split [11,47] is introduced as follows:

$$\overline{\boldsymbol{\sigma}} = \overline{\boldsymbol{\sigma}}^+ + \overline{\boldsymbol{\sigma}}^- \tag{7}$$

where the tensile effective stress and the compressive effective stress are

$$\begin{cases} \overline{\boldsymbol{\sigma}}^+ = \mathbb{P}^+ : \overline{\boldsymbol{\sigma}} = \sum_t H(\hat{\overline{\sigma}}_t)\hat{\overline{\sigma}}_t \boldsymbol{p}^{(t)} \otimes \boldsymbol{p}^{(t)} \\ \overline{\boldsymbol{\sigma}}^- = \mathbb{P}^- : \overline{\boldsymbol{\sigma}} = \sum_t [1 - H(\hat{\overline{\sigma}}_t)]\hat{\overline{\sigma}}_t \boldsymbol{p}^{(t)} \otimes \boldsymbol{p}^{(t)} \end{cases} \tag{8}$$

and the projective tensors

$$\begin{cases} \mathbb{P}^+ = \sum_t H(\hat{\overline{\sigma}}_t)\boldsymbol{p}^{(t)} \otimes \boldsymbol{p}^{(t)} \otimes \boldsymbol{p}^{(t)} \otimes \boldsymbol{p}^{(t)} \\ \mathbb{P}^- = \mathbb{I} - \mathbb{P}^+ \end{cases} \tag{9}$$

where $\hat{\overline{\sigma}}_t$ and $\boldsymbol{p}^{(t)}$ are the t-th eigenvalue and eigenvector of the effective stress tensor, respectively. And the Heaviside function reads

$$H(x) = \begin{cases} 0 & x \le 0 \\ 1 & x > 0 \end{cases} \tag{10}$$

As shown in Fig. 1, the eigen-based effective stress split defines the tensile stress state and the compressive stress state respectively. The projective tensors $\mathbb{P}^+$ and $\mathbb{P}^-$, which define the eigen-tensors of the fourth order damage tensor, are expressed by the principal directions of effective stress. Thus the proposed damage model is a kind of equivalent form to the rotating angle shear model [14] because the rotation of the principal effective stress yields the rotation of the principal damage.

The evolutions of the tensile damage D^+ and the compressive damage D^- should be governed by the corresponding stress states. Meanwhile, the irreversible thermodynamics suggests the energy conjugated force as the driven force (criterion) of the internal variable. Thus by proposing the expression of Helmholtz free energy (HFE)

$$\Psi = (1 - D^+)\Psi_0^+ + (1 - D^-)\Psi_0^- \tag{11}$$

the energy conjugated quantities of the tensile and the compressive damages, which are defined as the damage release rates, are

$$\begin{cases} Y^+ = -\frac{\partial \Psi}{\partial D^+} = \Psi_0^+ \\ Y^- = -\frac{\partial \Psi}{\partial D^-} = \Psi_0^- \end{cases} \tag{12}$$

The initial HFEs Ψ_0^+ and Ψ_0^- could be further split into the elastic part and the plastic part. We have

$$\begin{cases} \Psi_0^+ = \Psi_0^{e+} + \Psi_0^{p+} \\ \Psi_0^- = \Psi_0^{e-} + \Psi_0^{p-} \end{cases} \tag{13}$$

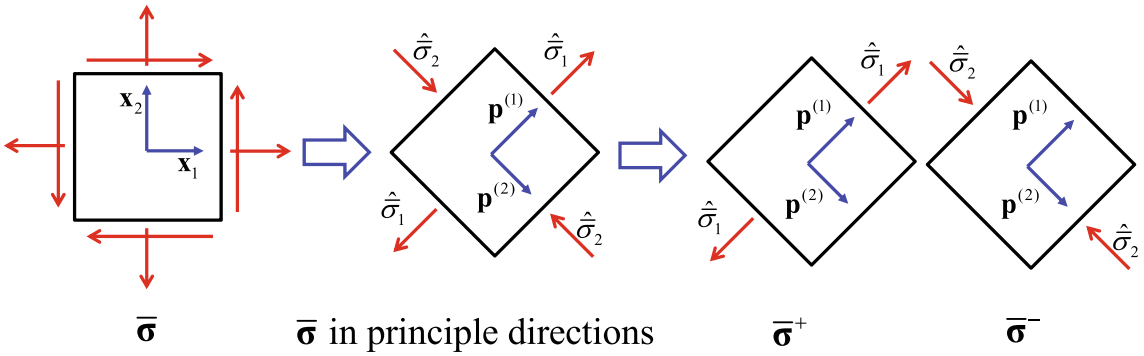

Fig. 1 Effective stress decomposition

The elastic parts

$$\Psi_0^{e\pm} = \frac{1}{2}\overline{\boldsymbol{\sigma}}^{\pm} : \boldsymbol{\epsilon}^e = \frac{1}{2}\overline{\boldsymbol{\sigma}}^{\pm} : \mathbb{E}_0^{-1} : \overline{\boldsymbol{\sigma}} \tag{14}$$

and the plastic parts [16]

$$\Psi_0^{p\pm} \approx \int \overline{\boldsymbol{\sigma}}^{\pm} : d\boldsymbol{\epsilon}^p \tag{15}$$

Wu et al. [47] neglected the tensile plastic HFE Ψ_0^{p+} and introduced the Drucker–Prager plastic model for the compressive HFE Ψ_0^{p-}. They derived the approximate explicit expressions of the damage release rates as follows

$$\begin{cases} Y^+ \approx \frac{1}{2E_0}\left[\frac{2(1+\nu_0)}{3}3\overline{J}_2^+ + \frac{1-2\nu_0}{3}(\overline{I}_1^+)^2 - \nu_0\overline{I}_1^+\overline{I}_1^-\right] \\ Y^- \approx b_0\left(\alpha\overline{I}_1^- + \sqrt{3\overline{J}_2^-}\right)^2 \end{cases} \tag{16}$$

where $\overline{I}_1^{\pm}$ are the first invariants of the tensile and the compressive effective stresses $\overline{\boldsymbol{\sigma}}^{\pm}$, respectively; and $\overline{J}_2^{\pm}$ are the second invariants of $\overline{\boldsymbol{s}}^{\pm}$, which is the deviatoric components of effective stresses. E_0 and ν_0 are the Young's modulus and the Poisson's ratio of the initial undamaged material; and b_0 is also a material parameter. The parameter α is related to the biaxial strength increase as follows

$$\alpha = \frac{\frac{f_{bc}}{f_c} - 1}{2\frac{f_{bc}}{f_c} - 1} \tag{17}$$

where f_c and f_{bc} are the uniaxial compressive strength and the biaxial compressive strength, respectively. It is observed from Eq. (16) that the developed tensile damage release rate Y^+ is governed by the elastic energy and the developed compressive damage release rate Y^- is governed by the plastic energy.

Moreover, the damage evolutions are defined by the energy release rates as follows

$$D^{\pm} = G^{\pm}(r_Y^{\pm}),\ r_Y^{\pm} = \max_{\tau\in[0,t]}\{Y^{\pm}(\tau)\} \tag{18}$$

where the monotonic functions $G^{\pm}(\cdot)$ are the damage evolution functions; and the damage thresholds $r_Y^{\pm}$ denote the maximum values of $Y^{\pm}$ throughout the whole loading process $[0, t]$. Based on the damage release rate dependent damage evolution and the damage consistent condition, Li and Ren [23] further developed the damage evolution driven by the energy equivalent strain as follows

$$D^{\pm} = G^{\pm}(r_e^{\pm}),\ r_e^{\pm} = \max_{\tau\in[0,t]}\{\overline{\epsilon}^{e\pm}(\tau)\} \tag{19}$$

where the energy equivalent strain

$$\begin{cases} \overline{\epsilon}^{e+} = \sqrt{\frac{2Y^+}{E_0}} \\ \overline{\epsilon}^{e-} = \frac{1}{E_0(1-\alpha)}\sqrt{\frac{Y^-}{b_0}} \end{cases} \tag{20}$$

Under uniaxial loading, the energy equivalent strains are reduced to the uniaxial strain while the damage evolutions are reduced to the uniaxial damage evolution as follows

$$D^{\pm} = G^{\pm}(r_e^{\pm}),\ r_e^{\pm} = \max_{\tau\in[0,t]}(\epsilon_{\tau}^{e\pm}) \tag{21}$$

It is observed that the multiaxial damage evolution Eq. (19) is consistent with the uniaxial damage evolution Eq. (21). The damage evolution functions $G^{\pm}(\cdot)$ could be determined by the uniaxial testing data or the theoretical development in the sub-scale.

The evolutionary models for the damage and the plasticity are developed in Chapter 3 and Chapter 4, respectively.

3 Damage evolution

To consider the material rate-sensitivity, the rate dependent damage evolutions could be developed based on the inviscid damage evolutions shown in Eq. (19). By introducing the rate-dependent energy equivalent strain $\overline{\epsilon}_r^{e\pm}$, the rate-dependent damage evolutions are

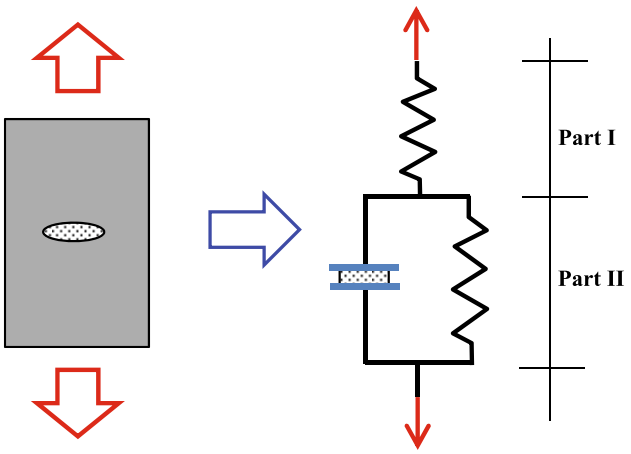

Fig. 2 Physical based rate-dependent model

$$\begin{cases} D^{\pm} = G^{\pm}(r_d^{\pm}) \\ r_d^{\pm} = \max_{\tau\in[0,t]}\{\bar{\epsilon}_r^{e\pm}(\tau)\} \\ \mathcal{R}^{\pm}(\bar{\epsilon}_r^{e\pm}, \dot{\bar{\epsilon}}_r^{e\pm}, \bar{\epsilon}^{e\pm}, \dot{\bar{\epsilon}}^{e\pm}) = 0 \end{cases} \tag{22}$$

Based on the Perzyna's theory [30], Ren and Li [32] proposed the phenomenological expression of the differential operator $\mathcal{R}^{\pm}$. In the present work, an alternative model is proposed based on the concept of Stefan effect.

Stefan [42] and Reynolds [34] investigated the problem of two separating plates with a thin viscous film in-between. The solution of this problem indicated the linear dependencies between the applied forces and the separating velocity of the plates. Thereafter, the findings was defined as Stefan effects and widely used to describe the material rate-dependencies. The derivation of the Stefan effect could be found in Appendix A. In the proposed model, we consider that the material rate-sensitivity comes from the Stefan effect.

We assume that the rate-dependency is induced by the water (including the void water and the crystal water) within concrete. As shown in Fig. 2, two parts are considered in the model. Part I represents the elastic part of concrete specimen and Part II is the combination of the solid matrix and the viscous fluid. We obtain the following equation after analyzing the model shown in Fig. 2.

$$\begin{cases} \epsilon_1 = \frac{\sigma}{E_1} \\ \epsilon_2 = \frac{\sigma-\sigma_v}{E_2} \end{cases} \tag{23}$$

where σ is the uniaxial stress; ϵ_1 and ϵ_2 are the strains of Part I and Part II, respectively; and E_1 and E_2 are the elastic parameters of Part I and Part II, respectively. Based on the discussion of the Stefan effect in Appendix A, the viscous stress representing the rate effect of the model could be expressed as follows

$$\sigma_v = A\dot{\epsilon}_2 \tag{24}$$

The viscous coefficient A has been defined in Appendix A. Based on Eqs. (23) and (24), the overall strain of the model could be expressed as

$$\epsilon_r = \epsilon_1 + \epsilon_2 = \sigma\left(\frac{1}{E_1} + \frac{1}{E_2}\right) - \frac{\sigma_v}{E_2} \tag{25}$$

For the quasi-static loading, we have $\sigma_v \to 0$. Eq. (25) reduces to

$$\epsilon = \epsilon_1 + \epsilon_2 = \frac{\sigma}{E_0} \tag{26}$$

where $\frac{1}{E_0} = \frac{1}{E_1} + \frac{1}{E_2}$ defines the equivalent uniaxial elastic parameters E_0. It is also observed that ϵ_r is the rate dependent strain of the system shown in Fig. 2 and ϵ is the quasi-static strain. And according to Eq. (25) we could further define $\epsilon_v = \frac{\sigma_v}{E_2}$ as the viscosity induced strain decrease. Manipulating Eqs. (23)– (26) yields the following first order differential system

$$\begin{cases} \gamma_a\dot{\epsilon}_2 + (\alpha_n + \beta_n)\epsilon_2 = \alpha_n\epsilon_r \\ \gamma_a\dot{\epsilon}_2 + \beta_n\epsilon_r = \beta_n\epsilon \end{cases} \tag{27}$$

where the coefficients

$$\gamma_a = \frac{A}{E_0},\ \alpha_n = 1+n,\ \beta_n = \frac{1+n}{n},\ n = \frac{E_1}{E_2} \tag{28}$$

By giving the static strain ϵ, the rate-dependent strain ϵ_r and the strain of Part II ϵ_2 could be solved by the dual system shown in Eq. (27). It is indicated that ϵ_r is needed to further calculate the rate-dependent damage, and particularly ϵ_2 is an internal variable which memorizes the strain history.

The numerical algorithm to solve Eq. (27) under general loading conditions will be developed in Chapter 5. The closed form solution of Eq. (27) reads

$$\begin{cases} \epsilon_2 = \epsilon_r - \frac{\beta_n\epsilon}{\alpha_n+\beta_n} \\ \epsilon_r = \frac{\beta_n e^{-\frac{\beta_n t}{\gamma_a}}}{\gamma_a(\alpha_n+\beta_n)}\int e^{\frac{\beta_n t}{\gamma_a}}\left[\gamma_a\dot{\epsilon} + (\alpha_n+\beta_n)\epsilon\right]dt + C_1 e^{-\frac{\beta_n t}{\gamma_a}} \end{cases} \tag{29}$$

where C_1 is a constant related to the initial conditions. Considering the constant rate loading $\epsilon = \dot{\epsilon}t$ and the initial condition ($\epsilon(0) = 0, \epsilon_r(0) = 0$), the solution Eq. (29) further gives

$$\epsilon_r = \epsilon - \epsilon_v \tag{30}$$

where the viscous strain

$$\epsilon_v = \frac{\alpha_n\gamma_a}{\beta_n(\alpha_n+\beta_n)}\left(1 - e^{-\frac{\beta_n t}{\gamma_a}}\right)\dot{\epsilon} \tag{31}$$

The closed form solution shown in Eqs. (30) and (31) could verify the simulating results of the numerical scheme.

The development of damage evolution function is refer to [17] and [23]. The stochastic damage evolution functions under static loading are expressed as follows

$$D = \int_0^1 H[\epsilon - \Delta(x)]dx \tag{32}$$

where $\Delta(x)$ is the 1-D micro-fracture strain random field; x is the spatial coordinate of the random field. And it is observed that ϵ is an constant subjected to spatial integration. By replacing the static strain ϵ with the dynamic strain ϵ_r, we have the rate-dependent stochastic damage evolution as follows

$$D = \int_0^1 H[\epsilon_r - \Delta(x)]dx \hat{=} G(\epsilon_r) \tag{33}$$

Consider that $\Delta(x)$ is a homogeneous log-normal random field. Let λ and ζ be two distribution parameters which denote the mean value and the standard deviation of the corresponding normal random variable $Z(x) = \ln \Delta(x)$, respectively. And the auto-correlation coefficient function for $Z(x)$ is as follows

$$\rho_z(y) = e^{-\xi|y|} \tag{34}$$

where ξ is the correlation parameter. Then the mean value and the standard deviation of damage evolutions expressed in Eq. (33) could be solved. The mean value reads

$$d = \mu_D = \Phi_i\left(\frac{\ln \epsilon_r - \lambda}{\zeta}\right) \hat{=} g(\epsilon_r) \tag{35}$$

and the standard deviation reads

$$V_D^2 = 2\int_0^1 (1-y)\Phi_{ii}\left(\frac{\ln \epsilon_r - \lambda}{\zeta}, \frac{\ln \epsilon_r - \lambda}{\zeta}\middle| \rho_z(y)\right) \mathrm{d}y - \mu_D^2 \tag{36}$$

where functions Φ_i and Φ_{ii} are the cumulative probability functions of the 1-D and the 2-D standard normal distributions, respectively. For the deterministic analysis, the mean value evolution Eq. (35) is adopted and the damage variable is denoted by the lower case variable d.

Before implementing the developed uniaxial rate-dependent damage evolutionary model [Eqs. (27)–(36)] into the multiaxial framework, the following aspects should be emphasized:

- Due to the essential differences between the behaviors of quasi-brittle materials under tension and compression, two groups of equations with similar expressions but different parameters are developed to reproduce the tensile damage and the compressive damage, respectively. And the superscripts $+$ and $-$ are adopted to denote the quantities related the tensile and the compressive damages as appropriate.
- The strains mentioned in the proposed method are refereed to the elastic strain. And the additional plastic strains will be modeled in the next section. By substituting the energy equivalent strain $\overline{\epsilon}^{e\pm}$ into Eqs. (27) as the static strain ϵ, the rate-dependent energy equivalent strain $\overline{\epsilon}_r^{e\pm}$ could be solved as ϵ_r. Thereafter the dynamic damage thresholds $r_d^{\pm}$ could be determined by considering the maximum values of $\overline{\epsilon}_r^{e\pm}$ over the entire loading process. Further substituting $r_d^{\pm}$ into the damage evolution functions Eqs. (33) and (35), the stochastic as well as the deterministic damages could be obtained.

4 Multi-variable plasticity

As discussed in Chapter 2, the T-ESP exhibits numbers of deficiencies in application. Hence a phenomenological model to describe the ESP is developed in the present chapter.

On one hand, the proposed phenomenological plastic model should be also defined in the effective stress space to take the advantage of the ESP. On the other hand, the plastic strain is usually defined as a function of strain in experimental studies. Thus we consider that the evolution of plastic strain is proportional to the evolution of elastic strain, which is closely related to the effective stress. One obtains

$$\dot{\boldsymbol{\epsilon}}^p = f_p \dot{\boldsymbol{\epsilon}}^e \tag{37}$$

Besides the damage, the evolutions of plastic strain are also rather different under tension and compression. Thus the split of plastic strain rate is introduced as follows

$$\begin{cases} \dot{\boldsymbol{\epsilon}}^p = \dot{\boldsymbol{\epsilon}}^{p+} + \dot{\boldsymbol{\epsilon}}^{p-} \\ \dot{\boldsymbol{\epsilon}}^{p+} = f_p^+ \dot{\boldsymbol{\epsilon}}^{e+} = f_p^+ \mathbb{E}_0^{-1} : \dot{\tilde{\boldsymbol{\sigma}}}^+ \\ \dot{\boldsymbol{\epsilon}}^{p-} = f_p^- \dot{\boldsymbol{\epsilon}}^{e-} = f_p^- \mathbb{E}_0^{-1} : \dot{\tilde{\boldsymbol{\sigma}}}^- \end{cases} \tag{38}$$

The scalars $f_p^{\pm}$ are considered as functions of the corresponding damage variables $D^{\pm}$. We define the plastic theory shown in Eq. (38) as multi-variable plasticity because more than one plastic strain tensors are considered. By systematic investigations of experimental data, we propose the following expressions

$$f_p^{\pm} = f_p^{\pm}(\dot{D}^{\pm}, D^{\pm}) = H(\dot{D}^{\pm})\xi_p^{\pm}(D^{\pm})^{n_p^{\pm}} \tag{39}$$

where $\xi_p^{\pm}$ and $n_p^{\pm}$ are material parameters fitted by the experimental data; and the Heaviside function $H(\cdot)$ defines the associate evolutions between damage and plasticity. As discussed in Chapter 3, the inevitable randomness of damages could be described by a random field. Thus the plastic evolutions are also random and related to the stochastic damage evolutions. On the other hand, the coupling between the randomness of damage and the nonlinearity of plastic evolution yields extremely complicated solutions of the total stress strain relationship Eq. (1). Thus a reduced form of the plastic evolution Eq. (39) is proposed as follows by using the mean values of damage (denoted by the lower case character $d^{\pm}$).

$$f_p^{\pm} = f_p^{\pm}(\dot{D}^{\pm}, d^{\pm}) = H(\dot{D}^{\pm})\xi_p^{\pm}(d^{\pm})^{n_p^{\pm}} \tag{40}$$

By combining Eqs. (38) and (40), we obtain the governing equation of plastic evolution as follows

$$\begin{aligned}\dot{\boldsymbol{\epsilon}}^{p} &= H(\dot{D}^{+})\xi_{p}^{+}(d^{+})^{n_{p}^{+}}\mathbb{E}_{0}^{-1}:\dot{\tilde{\boldsymbol{\sigma}}}^{+} \\ &\quad + H(\dot{D}^{-})\xi_{p}^{-}(d^{-})^{n_{p}^{-}}\mathbb{E}_{0}^{-1}:\dot{\tilde{\boldsymbol{\sigma}}}^{-} \\ &= H(\dot{D}^{+})\xi_{p}^{+}(d^{+})^{n_{p}^{+}}\mathbb{E}_{0}^{-1}:\mathbb{Q}^{+}:\dot{\tilde{\boldsymbol{\sigma}}} \\ &\quad + H(\dot{D}^{-})\xi_{p}^{-}(d^{-})^{n_{p}^{-}}\mathbb{E}_{0}^{-1}:\mathbb{Q}^{-}:\dot{\tilde{\boldsymbol{\sigma}}}\end{aligned} \tag{41}$$

The definition of the effective stress rate projective tensors [11] is

$$\dot{\tilde{\boldsymbol{\sigma}}}^{\pm} = \mathbb{Q}^{\pm}:\dot{\tilde{\boldsymbol{\sigma}}} \tag{42}$$

It is clear that $\mathbb{Q}^{\pm}$ are rather different from the effective stress projective tensors $\mathbb{P}^{\pm}$. By referring to [47], the present paper gives the expression of them as follows

$$\begin{cases}\mathbb{Q}^{+} = \mathbb{P}^{+} + 2\sum 3_{t=1}\sum_{s=1}^{t}\frac{\langle\hat{\tilde{\sigma}}_{t}\rangle-\langle\hat{\tilde{\sigma}}_{s}\rangle}{\hat{\tilde{\sigma}}_{t}-\hat{\tilde{\sigma}}_{s}}\boldsymbol{p}^{(ts)}\otimes\boldsymbol{p}^{(ts)} \\ \mathbb{Q}^{-} = \mathbb{I}-\mathbb{Q}^{+}\end{cases} \tag{43}$$

where the second order symmetric tensor

$$\boldsymbol{p}^{(ts)} = \frac{1}{2}(\boldsymbol{p}^{(t)}\otimes\boldsymbol{p}^{(s)} + \boldsymbol{p}^{(t)}\otimes\boldsymbol{p}^{(s)}) \tag{44}$$

where the superscripts t and s in brackets denote the orders of the eigenvalues or the eigenvectors of the effective stress. And the Macaulay brackets

$$\langle x\rangle = \frac{|x|+x}{2} \tag{45}$$

To determine the elasoplastic tangential stiffness tensor, the differentiation of Eq. (2) yields

$$\dot{\tilde{\boldsymbol{\sigma}}} = \mathbb{E}_{0}:(\dot{\boldsymbol{\epsilon}}-\dot{\boldsymbol{\epsilon}}^{p}) \tag{46}$$

Combining Eqs. (41) and (46) gives

$$\begin{aligned}&\left[\mathbb{I} + H(\dot{D}^{+})\xi_{p}^{+}(d^{+})^{n_{p}^{+}}\mathbb{Q}^{+} + H(\dot{D}^{-})\xi_{p}^{-}(d^{-})^{n_{p}^{-}}\mathbb{Q}^{-}\right]:\dot{\tilde{\boldsymbol{\sigma}}} \\ &= \mathbb{E}_{0}:\dot{\boldsymbol{\epsilon}}\end{aligned} \tag{47}$$

Hence the elasoplastic tangential stiffness tensor reads

$$\begin{aligned}\mathbb{E}^{ep} &= \Big[\mathbb{I} + H(\dot{D}^{+})\xi_{p}^{+}(d^{+})^{n_{p}^{+}}\mathbb{Q}^{+} \\ &\quad + H(\dot{D}^{-})\xi_{p}^{-}(d^{-})^{n_{p}^{-}}\mathbb{Q}^{-}\Big]^{-1}:\mathbb{E}_{0}\end{aligned} \tag{48}$$

The rate-dependency of plasticity is not explicitly included in the proposed plastic model. However, due to the rate dependencies of damage evolutions, the plastic evolution is technically related to the strain rates. Furthermore, although the linear rate-dependency is defined by Eq. (27), the proposed plastic damage model exhibits strong nonlinearities dependent to the strain rate. The reason could refer to the nonlinear dependency between the damage and the plasticity proposed in the present work.

Further define the plastic stress and plastic stress rates as follows

$$\begin{cases}\boldsymbol{\sigma}^{p\pm} = \mathbb{E}_{0}:\boldsymbol{\epsilon}^{p\pm} \\ \dot{\boldsymbol{\sigma}}^{p\pm} = \mathbb{E}_{0}:\dot{\boldsymbol{\epsilon}}^{p\pm}\end{cases} \tag{49}$$

Recall Eqs. (38) and (40), we have

$$\dot{\boldsymbol{\sigma}}^{p\pm} = H(\dot{D}^{\pm})\xi_{p}^{\pm}(d^{\pm})^{n_{p}^{\pm}}\dot{\tilde{\boldsymbol{\sigma}}}^{\pm} \tag{50}$$

Thus Eq. (46) could be recast into the following form

$$\dot{\tilde{\boldsymbol{\sigma}}} = \mathbb{E}_{0}:\dot{\boldsymbol{\epsilon}} - \dot{\boldsymbol{\sigma}}^{p+} - \dot{\boldsymbol{\sigma}}^{p-} \tag{51}$$

Theoretically, the plastic stress $\boldsymbol{\sigma}^{p\pm}$ are equivalent to the plastic strain $\boldsymbol{\epsilon}^{p\pm}$. But Eq. (51) suggests that $\boldsymbol{\sigma}^{p\pm}$ works better with the effective stress and yields very concise expressions. Thus the numerical scheme is developed in the form of plastic stress.

5 Numerical scheme

At each integration point of the structural finite element model, the unknown stress increments should be calculated by the constitutive model during each time-step. As shown in the previous chapters, the proposed constitutive relationship defines a strong nonlinear system made up of a set of coupled nonlinear equations. Thus the numerical implementation of the proposed model should be carefully considered to guarantee the accuracy and the stability of the structural simulation. The existing numerical schemes for the computation of the material inelasticity could be concluded as follows:

- The implicit methods are generally unconditionally stable. Hence a relatively long time step could be adopted so that less numbers of time step is needed. And another attractive aspect indicates that the results of the implicit method automatically satisfy the yield condition. On the other hand, these methods need iterations to solve the resulting implicit equations. The internal iterations may diverge for the strain softening problem or other ill-conditioned cases. And the second derivatives of the yield functions, which are rather complicated for the general forms of the yield functions, are required to calculate the algorithm consistent tangential tensor.
- The explicit methods are conditionally stable. Thus they require rather small time steps to avoid intolerable errors, so that a large number of time steps are needed. And the results of these methods may not satisfy the yield condition to the predefined tolerance. However, the explicit methods offer an extremely simple but robust computations in each time step. No iteration is needed and the order of derivatives remains to one. Moreover, the explicit methods fit the parallel code very well and is able to achieve excellent efficiency for the parallel computation.

In the present paper, an explicit scheme is developed to implement the proposed rate-dependent damage–plasticity model. Denote the subscript form x_k as the quantities at the k-th time step. And the finite difference is defined by $\Delta x_k = x_{k+1} - x_k$. By giving the values of the state variables and the internal variables in the k-th time step and also the strain in the (k+1)-th step, the proposed scheme approaches the values of the state variables and the internal variables in the (k+1)-th step.

We start with the elastic trial. By freezing the evolutions of plasticity and damage, the trial solution of the effective stress as follows

$$\overline{\boldsymbol{\sigma}}^{\text{trial}}_{k+1} = \mathbb{E}_0 : \boldsymbol{\epsilon}_{k+1} - \boldsymbol{\sigma}^p_k \tag{52}$$

Then the trial solutions of the damage energy release rates $(Y^{\pm})^{\text{trial}}_{k+1}$ and the energy equivalent strains $(\overline{\epsilon}^{e\pm})^{\text{trial}}_{k+1}$ could be explicitly determined. The rate dependent energy equivalent strains could be solved by the finite difference discretization of Eqs. (27) as follows

$$\begin{cases} \gamma^{\pm}_a \left[(\overline{\epsilon}^{\pm}_2)_{k+1} - (\overline{\epsilon}^{\pm}_2)_k\right] \\ \quad + (\alpha^{\pm}_n + \beta^{\pm}_n)(\overline{\epsilon}^{\pm}_2)_{k+1}\Delta t_k = \alpha^{\pm}_n (\overline{\epsilon}^{e\pm}_r)_{k+1}\Delta t_k \\ \gamma^{\pm}_a \left[(\overline{\epsilon}^{\pm}_2)_{k+1} - (\overline{\epsilon}^{\pm}_2)_k\right] \\ \quad + \beta^{\pm}_n (\overline{\epsilon}^{e\pm}_r)_{k+1}\Delta t_k = \beta^{\pm}_n (\overline{\epsilon}^{e\pm})_{k+1}\Delta t_k \end{cases} \tag{53}$$

Cast into matrix expression, we obtain

$$\begin{bmatrix} \gamma^{\pm}_a + (\alpha^{\pm}_n + \beta^{\pm}_n)\Delta t_k & -\alpha^{\pm}_n \Delta t_k \\ \gamma^{\pm}_a & \beta^{\pm}_n \Delta t_k \end{bmatrix} \begin{Bmatrix} (\overline{\epsilon}^{\pm}_2)_{k+1} \\ (\overline{\epsilon}^{e\pm}_r)_{k+1} \end{Bmatrix} = \begin{Bmatrix} \gamma^{\pm}_a (\overline{\epsilon}^{\pm}_2)_k \\ \gamma^{\pm}_a (\overline{\epsilon}^{\pm}_2)_k + \beta^{\pm}_n (\overline{\epsilon}^{e\pm})_{k+1}\Delta t_k \end{Bmatrix} \tag{54}$$

An inversion gives

$$\begin{Bmatrix} (\overline{\epsilon}^{\pm}_2)_{k+1} \\ (\overline{\epsilon}^{e\pm}_r)_{k+1} \end{Bmatrix} = \begin{bmatrix} \frac{\gamma^{\pm}_a}{\gamma^{\pm}_a + \beta^{\pm}_n \Delta t_k} & \frac{\alpha^{\pm}_n \beta^{\pm}_n \Delta t_k}{(\alpha^{\pm}_n + \beta^{\pm}_n)(\gamma^{\pm}_a + \beta^{\pm}_n \Delta t_k)} \\ \frac{\gamma^{\pm}_a}{\gamma^{\pm}_a + \beta^{\pm}_n \Delta t_k} & \frac{\gamma^{\pm}_a \beta^{\pm}_n + (\alpha^{\pm}_n + \beta^{\pm}_n)\Delta t_k \beta^{\pm}_n}{(\alpha^{\pm}_n + \beta^{\pm}_n)(\gamma^{\pm}_a + \beta^{\pm}_n \Delta t_k)} \end{bmatrix} \begin{Bmatrix} (\overline{\epsilon}^{\pm}_2)_k \\ (\overline{\epsilon}^{e\pm})_{k+1} \end{Bmatrix} \tag{55}$$

Substituting the trial energy equivalent strains $(\overline{\epsilon}^{e\pm})^{\text{trial}}_{k+1}$ into the discrete system Eq. (54), the trial rate-dependent energy equivalent strains $(\overline{\epsilon}^{e\pm}_r)^{\text{trial}}_{k+1}$ and the trial internal energy equivalent strains $(\overline{\epsilon}^{\pm}_2)^{\text{trial}}_{k+1}$ could be solved. Thus the trial damage criteria gives

$$(R^{\pm})^{\text{trial}}_{k+1} = |(\overline{\epsilon}^{e\pm}_r)^{\text{trial}}_{k+1}| - |(r^{\pm}_d)_k| \tag{56}$$

If

$$(R^{\pm})^{\text{trial}}_{k+1} \le 0 \tag{57}$$

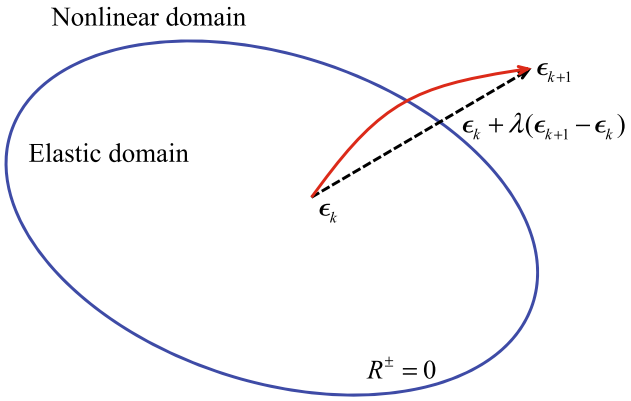

Fig. 3 Damage criterion intersection

the elastic state holds. We obtain

$$\begin{aligned} &D^{\pm}_{k+1} = D^{\pm}_k,\ \boldsymbol{\sigma}^p_{k+1} = \boldsymbol{\sigma}^p_k \\ &(r^{\pm}_d)_{k+1} = (r^{\pm}_d)_k,\ (\overline{\epsilon}^{\pm}_2)_{k+1} = (\overline{\epsilon}^{\pm}_2)_k,\ \overline{\boldsymbol{\sigma}}_{k+1} = \overline{\boldsymbol{\sigma}}^{\text{trial}}_{k+1} \\ &\boldsymbol{\sigma}_{k+1} = \overline{\boldsymbol{\sigma}}_{k+1} - D^{+}_{k+1}\overline{\boldsymbol{\sigma}}^{+}_{k+1} - D^{-}_{k+1}\overline{\boldsymbol{\sigma}}^{-}_{k+1} \end{aligned} \tag{58}$$

For $(R^{\pm})^{\text{trial}}_{k+1} > 0$, the damage and the plasticity evolve. The explicit methods usually require special attentions to the case that the effective stress point changes from the elastic stage to the nonlinear stage (Fig. 3).

The current time-step includes an elastic sub-step following by a nonlinear sub-step. And different governing equations hold for different sub-steps, respectively. If the state variables in the nonlinear domain are directly predicted by the starting point located in the elastic domain, the abnormal errors would happen during the calculation. Thus the transition point should be determined beforehand. Then the integration could be performed through two sub-steps with corresponding starting points and governing equations. As the time increments are usually very small for the explicit schemes to guarantee the overall numerical stability, we could linearize the load path within the time increment into a straight path without loss of much accuracy. Sloan et al. [39], Soan [40] systematically investigated the explicit methods for the plastic models and proposed the Pegasus algorithm to find the intersection point of a straight loading path. In the present work, the Pegasus algorithm developed for damage model is shown in Algorithm 1. Actually, the elastic sub-step could be also finished during the execution of the Pegasus algorithm with the damage and the plasticity remain unchanged.

By starting at the end of the elastic sub-step, we evaluate the evolutions of damage and plasticity based on the forward Euler scheme. By recalling Eqs. (47) and (48), the forward Euler scheme gives

$$\begin{aligned} \mathbb{T}^{ep}_{k+\lambda} : (\overline{\boldsymbol{\sigma}}_{k+1} - \overline{\boldsymbol{\sigma}}_{k+\lambda}) &= \mathbb{E}_0 : (\boldsymbol{\epsilon}_{k+1} - \boldsymbol{\epsilon}_{k+\lambda}) \\ &= \overline{\boldsymbol{\sigma}}^{\text{trial}}_{k+1} - \overline{\boldsymbol{\sigma}}_{k+\lambda} \end{aligned} \tag{59}$$

begin
  Initialization with
  $\lambda_0^{\pm} \leftarrow 0$; $\lambda_1^{\pm} \leftarrow 1$;
  $R_0^{\pm} \leftarrow |(\overline{\epsilon}_r^{e\pm})_k| - |(r_d^{\pm})_k|$; $R_1^{\pm} \leftarrow |(\overline{\epsilon}_r^{e\pm})_{k+1}^{\text{trial}}| - |(r_d^{\pm})_k|$;
  /*interations to solve the intersection point */
  for $i \leftarrow 1$ ***to*** MAXITS **do**
    $\lambda^{\pm} \leftarrow \lambda_1^{\pm} - \frac{R_1^{\pm}}{R_1^{\pm} - R_0^{\pm}}(\lambda_1^{\pm} - \lambda_0^{\pm})$;
    $\boldsymbol{\epsilon}_{k+\lambda^{\pm}} \leftarrow \boldsymbol{\epsilon}_k + \lambda^{\pm}(\boldsymbol{\epsilon}_{k+1} - \boldsymbol{\epsilon}_k)$;
    $t_{k+\lambda^{\pm}} \leftarrow t_k + \lambda^{\pm}(t_{k+1} - t_k)$;
    Calculate $(\overline{\epsilon}_r^{e\pm})_{k+\lambda^{\pm}}$ and $(\overline{\epsilon}_2^{e\pm})_{k+\lambda^{\pm}}$ by Eqs. (54);
    $R_{\lambda^{\pm}}^{\pm} \leftarrow |(\overline{\epsilon}_r^{e\pm})_{k+\lambda^{\pm}}| - |(r_d^{\pm})_k|$;
    if $|R_{\lambda^{\pm}}^{\pm}| \le$ RTOL **then**
      break;
    end
    if $R_{\lambda^{\pm}}^{\pm} R_0^{\pm} < 0$ **then**
      $\lambda_1^{\pm} \leftarrow \lambda^{\pm}$; $R_1^{\pm} \leftarrow R_{\lambda^{\pm}}^{\pm}$;
      else
        $\lambda_0^{\pm} \leftarrow \lambda^{\pm}$; $R_0^{\pm} \leftarrow R_{\lambda^{\pm}}^{\pm}$;
      end
    end
  end
  if $|R_{\lambda^{\pm}}^{\pm}| \le$ RTOL **then**
    $\overline{\boldsymbol{\sigma}}_{k+\lambda^{\pm}} \leftarrow \overline{\boldsymbol{\sigma}}_k + \mathbb{E}_0 : (\boldsymbol{\epsilon}_{k+\lambda^{\pm}} - \boldsymbol{\epsilon}_k)$;
    $\boldsymbol{\sigma}_{k+\lambda^{\pm}} \leftarrow \overline{\boldsymbol{\sigma}}_{k+\lambda^{\pm}} - D_k^{+}\overline{\boldsymbol{\sigma}}_{k+\lambda^{\pm}}^{+} - D_k^{-}\overline{\boldsymbol{\sigma}}_{k+\lambda^{\pm}}^{-}$;
    else
      exit with error message;
    end
  end
end

Algorithm 1: Pegasus algorithm

Further manipulation yields

$$\mathbb{T}_{k+\lambda}^{ep} : \overline{\boldsymbol{\sigma}}_{k+1} = \overline{\boldsymbol{\sigma}}_{k+1}^{\text{trial}} - (\mathbb{I} - \mathbb{T}_{k+\lambda}^{ep}) : \overline{\boldsymbol{\sigma}}_{k+\lambda} \tag{60}$$

where the fourth order tensor $\mathbb{T}^{ep}$ at the k-th step is

$$\mathbb{T}_{k+\lambda}^{ep} = \mathbb{I} + \theta_k^{p+}\mathbb{Q}_{k+\lambda}^{+} + \theta_k^{p-}\mathbb{Q}_{k+\lambda}^{-} \tag{61}$$

and the plastic factors are

$$\begin{aligned} \theta_k^{p+} &= H\left[(D^{+})_{k+1}^{\text{trial}} - D_k^{+}\right]\xi_p^{+}\left[d_k^{+}\right]^{n_p^{+}} \\ \theta_k^{p-} &= H\left[(D^{-})_{k+1}^{\text{trial}} - D_k^{-}\right]\xi_p^{-}\left[d_k^{-}\right]^{n_p^{-}} \end{aligned} \tag{62}$$

Recall Eq. (38), the plastic stress could be determined by

$$\begin{aligned} \boldsymbol{\sigma}_{k+1}^{p} = \boldsymbol{\sigma}_k^{p} &+ \theta_k^{p+}\left(\overline{\boldsymbol{\sigma}}_{k+1}^{+} - \overline{\boldsymbol{\sigma}}_{k+\lambda^{+}}^{+}\right) \\ &+ \theta_k^{p-}\left(\overline{\boldsymbol{\sigma}}_{k+1}^{-} - \overline{\boldsymbol{\sigma}}_{k+\lambda^{-}}^{-}\right) \end{aligned} \tag{63}$$

Then the energy equivalent strains $(\overline{\epsilon}_2^{\pm})_{k+1}$, $(\overline{\epsilon}^{\pm})_{k+1}$ and $(\overline{\epsilon}_r^{\pm})_{k+1}$ could be explicitly calculated. The damage criteria

$$\begin{cases} (r_d^{+})_{k+1} = \text{sgn}\{(r_d^{+})_k\}\max\{|(\overline{\epsilon}_r^{+})_{k+1}|, |(r_d^{+})_k|\} \\ (r_d^{-})_{k+1} = \text{sgn}\{(r_d^{-})_k\}\max\{|(\overline{\epsilon}_r^{-})_{k+1}|, |(r_d^{-})_k|\} \end{cases} \tag{64}$$

and the damage variables

$$\begin{cases} (D^{\pm})_{k+1} = G^{\pm}\left[(r_d^{\pm})_{k+1}\right] \\ (d^{\pm})_{k+1} = g^{\pm}\left[(r_d^{\pm})_{k+1}\right] \end{cases} \tag{65}$$

Finally the stress

$$\begin{aligned} \boldsymbol{\sigma}_{k+1} &= (\mathbb{I} - \mathbb{D}_{k+1}) : (\mathbb{E}_0 : \boldsymbol{\epsilon}_{k+1} - \boldsymbol{\sigma}_{k+1}^{p}) \\ &= (\mathbb{I} - \mathbb{D}_{k+1}) : (\overline{\boldsymbol{\sigma}}_{k+1}^{\text{trial}} + \boldsymbol{\sigma}_k^{p} - \boldsymbol{\sigma}_{k+1}^{p}) \end{aligned} \tag{66}$$

The time steps without elastic sub-step could be considered as the particular case of the elastic-nonlinear step with $\lambda^{\pm} = 0$.

The inconsistency induced by the extrapolation could be observed for the effective stress. Recalling Eq. (60), we find

$$\begin{aligned} \overline{\boldsymbol{\sigma}}_{k+1} &= (\mathbb{T}_{k+\lambda}^{ep})^{-1} : \left[\overline{\boldsymbol{\sigma}}_{k+1}^{\text{trial}} - (\mathbb{I} - \mathbb{T}_{k+\lambda}^{ep})\overline{\boldsymbol{\sigma}}_{k+\lambda}\right] \\ &\neq \mathbf{C}_0 : \boldsymbol{\epsilon}_{k+1} - \boldsymbol{\sigma}_{k+1}^{p} \hat{=} \tilde{\overline{\boldsymbol{\sigma}}}_{k+1} \end{aligned} \tag{67}$$

Thus the drift of damage criteria is

$$\begin{aligned} \tilde{R}_{k+1}^{\pm} &= |\overline{\epsilon}_r^{\pm}(\tilde{\overline{\boldsymbol{\sigma}}}_{k+1})| - |(r_d^{\pm})_{k+1}| \\ &= |\overline{\epsilon}_r^{\pm}(\tilde{\overline{\boldsymbol{\sigma}}}_{k+1})| - |r_d^{\pm}(\overline{\boldsymbol{\sigma}}_{k+1})| \neq 0 \end{aligned} \tag{68}$$

If the drift exceeds the tolerance, the global convergence of the explicit algorithm will be lost. Thus the criteria to control the global convergence of the numerical simulation should be put as follows

$$|\tilde{R}_{k+1}^{\pm}| \le \text{GTOL} \tag{69}$$

According to Reference [39], the suitable values of the global tolerance GTOL are typically in the range 10^{-6}–10^{-9}.

The complete explicit algorithm for the proposed damage–plasticity model is summarized in Algorithm 2.

6 Stability analysis

6.1 Physical stability analysis

The regularization operator $\mathcal{R}^{\pm}$ in Eq. (22) represents the material rate-dependency by slowing down the evolutions of damages $D^{\pm}$ under dynamic loading. It has been extensively investigated that the damage induced softening may yield strain localization, which is usually referred as the damage induced instability. On the other hand, the strain rate in the strain localized domain is basically larger than that in the rest part of solid. Thus the damage evolution in the strain localized domain would be slowed down much more when the rate-dependency is taken into account. This effect could be considered as a localization limiter. Needleman first showed that the material rate-dependency can remove the instability [26]. In the present work, the regularization operator $\mathcal{R}^{\pm}$ also

begin
  Initialization with $\boldsymbol{\sigma}_0, \overline{\boldsymbol{\sigma}}_0, \boldsymbol{\epsilon}_0, \boldsymbol{\sigma}_0^p, (\overline{\epsilon}_2^{\pm})_0, D_0^{\pm}, d_0^{\pm}, (r_d^{\pm})_0, \tilde{R}_0^{\pm}$;
  for $k \leftarrow 0$ ***to*** Nk **do**
    /*elastic trial */
    $\overline{\boldsymbol{\sigma}}_{k+1}^{\text{trial}} \leftarrow \mathbb{E}_0 : \boldsymbol{\epsilon}_{k+1} - \boldsymbol{\sigma}_k^p$;
    Calculate $(\overline{\epsilon}^{e\pm})_{k+1}^{\text{trial}}$;
    Calculate $(\overline{\epsilon}_r^{e\pm})_{k+1}^{\text{trial}}$ and $(\overline{\epsilon}_2^{e\pm})_{k+1}^{\text{trial}}$ by Eqs.(54);
    $(R^{\pm})_{k+1}^{\text{trial}} \leftarrow |(\overline{\epsilon}_r^{e\pm})_{k+1}^{\text{trial}}| - |(r_d^{\pm})_k|$;
    if $(R^{\pm})_{k+1}^{\text{trial}} \leq 0$ **then**
      /*pure elastic step */
      $D_{k+1}^{\pm} \leftarrow D_k^{\pm}$; $\boldsymbol{\sigma}_{k+1}^p \leftarrow \boldsymbol{\sigma}_k^p$; $(r_d^{\pm})_{k+1} \leftarrow (r_d^{\pm})_k$;
      $(\overline{\epsilon}_2^{\pm})_{k+1} \leftarrow (\overline{\epsilon}_2^{\pm})_{k+1}^{\text{trial}}$; $\overline{\boldsymbol{\sigma}}_{k+1} \leftarrow \overline{\boldsymbol{\sigma}}_{k+1}^{\text{trial}}$;
      $\boldsymbol{\sigma}_{k+1} \leftarrow \overline{\boldsymbol{\sigma}}_{k+1} - D_{k+1}^{+}\overline{\boldsymbol{\sigma}}_{k+1}^{+} - D_{k+1}^{-}\overline{\boldsymbol{\sigma}}_{k+1}^{-}$;
      $\tilde{R}_{k+1}^{\pm} \leftarrow (R^{\pm})_{k+1}^{\text{trial}}$;
      return ;
    end
    /*Nonlinear correction */
    if $\tilde{R}_k^{\pm} < -\text{GTOL}$ **then**
      Perform Algorithm 1 to determine $\lambda^{\pm}$;
      else
        $\lambda^{\pm} \leftarrow 0$;
      end
    end
    $\overline{\boldsymbol{\sigma}}_{k+1} \leftarrow (\mathbb{T}_{k+\lambda}^{ep})^{-1} : \left[\overline{\boldsymbol{\sigma}}_{k+1}^{\text{trial}} - (\mathbb{I} - \mathbb{T}_{k+\lambda}^{ep})\overline{\boldsymbol{\sigma}}_{k+\lambda}\right]$;
    $\boldsymbol{\sigma}_{k+1}^p \leftarrow \boldsymbol{\sigma}_k^p + \theta_k^{p+}\left(\overline{\boldsymbol{\sigma}}_{k+1}^{+} - \overline{\boldsymbol{\sigma}}_{k+\lambda^+}^{+}\right) + \theta_k^{p-}\left(\overline{\boldsymbol{\sigma}}_{k+1}^{-} - \overline{\boldsymbol{\sigma}}_{k+\lambda^-}^{-}\right)$;
    $(r_d^{+})_{k+1} \leftarrow \text{sgn}\{(r_d^{+})_k\}\max\{|(\overline{\epsilon}_r^{+})_{k+1}|, |(r_d^{+})_k|\}$;
    $(r_d^{-})_{k+1} \leftarrow \text{sgn}\{(r_d^{-})_k\}\max\{|(\overline{\epsilon}_r^{-})_{k+1}|, |(r_d^{-})_k|\}$;
    $(D^{\pm})_{k+1} \leftarrow G^{\pm}\left[(r_d^{\pm})_{k+1}\right]$; $(d^{\pm})_{k+1} \leftarrow g^{\pm}\left[(r_d^{\pm})_{k+1}\right]$;
    $\boldsymbol{\sigma}_{k+1} \leftarrow (\mathbb{I} - \mathbb{D}_{k+1}) : (\mathbb{E}_0 : \boldsymbol{\epsilon}_{k+1} - \boldsymbol{\sigma}_{k+1}^p)$;
    $\tilde{\overline{\boldsymbol{\sigma}}}_{k+1} \leftarrow \mathbb{E}_0 : \boldsymbol{\epsilon}_{k+1} - \boldsymbol{\sigma}_{k+1}^p$;
    $\tilde{R}_{k+1}^{\pm} \leftarrow |\overline{\epsilon}_r^{\pm}(\tilde{\overline{\boldsymbol{\sigma}}}_{k+1})| - |r_d^{\pm}(\overline{\boldsymbol{\sigma}}_{k+1})|$;
    /*check global convergence */
    if $|\tilde{R}_{k+1}^{\pm}| > \text{GTOL}$ **then**
      exit with error message;
    end
  end
end

Algorithm 2: Explicit algorithm

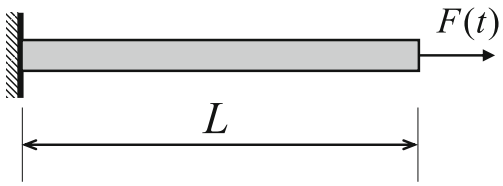

Fig. 4 Uniaxial bar problem in dynamic tensile

introduces a kind of non-locality for the spatial damage propagation, which may relieve the instability in the simulation of softening solids.

For simplicity, researchers [5,26,27,46] usually investigated the stability of the dynamically damaged system based on the uniaxial bar problem in tension, as shown in Fig. 4.

The equation of motion for the uniaxial bar problem reads

$$\frac{\partial \sigma}{\partial x} = \rho \frac{\partial^2 u}{\partial t^2} \tag{70}$$

with ρ the density of the material, σ the axial stress and u the axial displacement, x and t are spatial and temporal coordinates, respectively.

The equation of continuity reads

$$\epsilon = \frac{\partial u}{\partial x} \tag{71}$$

where ϵ denotes the uniaxial strain.

And the constitutive equation in 1-D is

$$\sigma = (1 - D)E_0(\epsilon - \epsilon^p) \tag{72}$$

where D is the uniaxial damage, E_0 is the undamaged Young's modulus, and ϵ^p is the plastic strain. For simplicity, we only consider the tensile loading bar and neglect the compressive damage in this discussion.

For the rate independent system, the damage are directly defined as the function of uniaxial elastic strain ϵ^e, we have

$$D = G(\epsilon^e)\ , \quad \epsilon^e = \epsilon - \epsilon^p \tag{73}$$

Moreover, the differentiation of Eq. (72) gives

$$\frac{\partial \sigma}{\partial x} = (1 - D - D'\epsilon^e)E_0\left(\frac{\partial \epsilon}{\partial x} - \frac{\partial \epsilon^p}{\partial x}\right) \tag{74}$$

Recalling the plastic model proposed in the former part, we have the standard first order expression of the governing equations for the rate independent system as follows

$$\begin{cases} (1 - D - D'\epsilon^e)E_0\left(\frac{\partial \epsilon}{\partial x} - \frac{\partial \epsilon^p}{\partial x}\right) - \rho\frac{\partial v}{\partial t} = 0 \\ \frac{\partial \epsilon}{\partial t} - \frac{\partial v}{\partial x} = 0 \\ f_p(D)\frac{\partial \epsilon}{\partial t} - [1 + f_p(D)]\frac{\partial \epsilon^p}{\partial t} = 0 \end{cases} \tag{75}$$

where the velocity $v = \frac{\partial u}{\partial t}$.

Consider the strain rate dependent damage evolutions, we have the damage evolution

$$D = G(\epsilon_r) \tag{76}$$

The rate dependent strain ϵ_r is governed by Eq. (27) with the total strain ϵ replaced by the elastic strain ϵ^e. In this case, the differentiation of Eq. (72) gives

$$\frac{\partial \sigma}{\partial x} = (1 - D)E_0\left(\frac{\partial \epsilon}{\partial x} - \frac{\partial \epsilon^p}{\partial x}\right) - D'E_0\frac{\partial \epsilon_r}{\partial x} \tag{77}$$

Therefore, the standard first order expression of the governing equations for the rate dependent system is as follows

$$\begin{cases} (1 - D)E_0\left(\frac{\partial \epsilon}{\partial x} - \frac{\partial \epsilon^p}{\partial x}\right) - D'E_0\epsilon^e\frac{\partial \epsilon_r}{\partial x} - \rho\frac{\partial v}{\partial t} = 0 \\ \frac{\partial \epsilon}{\partial t} - \frac{\partial v}{\partial x} = 0 \\ f_p(D)\frac{\partial \epsilon}{\partial t} - [1 + f_p(D)]\frac{\partial \epsilon^p}{\partial t} = 0 \\ \gamma_a\frac{\partial e_2}{\partial t} - \alpha_n\frac{\partial \epsilon_r}{\partial t} = -(\alpha_n + \beta_n)e_2 \\ \gamma_a\frac{\partial e_2}{\partial t} + \beta_n\frac{\partial \epsilon_r}{\partial t} - \beta_n\left(\frac{\partial \epsilon}{\partial t} - \frac{\partial \epsilon^p}{\partial t}\right) = 0 \end{cases} \tag{78}$$

where $e_2 = \frac{\partial \epsilon_2}{\partial t}$.

According to the theory of partial differential equation [29], the quasi-linear PDE could be expressed in the following form

$$\mathbf{P}(\mathbf{U})\frac{\partial \mathbf{U}}{\partial t} + \mathbf{Q}(\mathbf{U})\frac{\partial \mathbf{U}}{\partial x} = \mathbf{R}(\mathbf{U}) \tag{79}$$

Consider the generalized eigenproblem as follows

$$\mathbf{W}^{\mathrm{T}}(\mathbf{P} - \lambda\mathbf{Q}) = \mathbf{0}^{\mathrm{T}} \;\Rightarrow\; |\mathbf{P} - \lambda\mathbf{Q}| = 0 \tag{80}$$

Eq. (79) is hyperbolic if all the eigenvalues of Eq. (80) are real, which means the travelling wave occurs within the 1-D bar. On the other hand, if the complex eigenvalues are solved for Eq. (80), the wave could not travel within the bar and the deformation would concentrate in a local part [5,46]. Then the system loses its stability and the strain localization occurs.

By solving the eigenvalue problem for the rate independent system expressed in Eq. (75), we have the following expression of eigenvalues:

$$\begin{cases} \lambda = \pm\sqrt{\frac{\rho}{\frac{\partial\sigma}{\partial\epsilon}}} \\ \frac{\partial\sigma}{\partial\epsilon} = \frac{(1-D-D'\epsilon^e)E_0}{1+f_p(D)} \end{cases} \tag{81}$$

It is observed from Eq. (81) that the stability of the rate independent system Eq. (75) is governed by the tangential stiffness $\frac{\partial\sigma}{\partial\epsilon}$. If the material appears to be softening, the negative tangential stiffness leads to the loss of stability. This conclusion also agrees with the celebrated work of Bazant and Belytschko [2].

The eigenvalues of the the rate-dependent system expressed by Eq. (78) could solved as follows

$$\begin{cases} \lambda = \pm\sqrt{\frac{\rho}{\tilde{E}}} \\ \tilde{E} = \frac{\left(1-D-\frac{\beta}{\alpha+\beta}D'\epsilon^e\right)E_0}{[1+f_p(D)]\gamma} \end{cases} \tag{82}$$

A comparison between Eqs. (81) and (82) gives

$$1 - D - \frac{\beta}{\alpha+\beta}D'\epsilon^e > 1 - D - D'\epsilon^e \tag{83}$$

Thus we could conclude that the rate-dependent system expressed by Eq. (78) is more stable than the rate independent system expressed in Eq. (75). On the other hand, Eq. (78) is conditionally stable, which means the instability could be relieved but not be totally removed by the rate-dependence model introduced in the present work. The further improvements of the stability is undoubtedly an interesting topic, and the next step-forward in this direction will be reported in our forthcoming works.

6.2 Numerical stability analysis

Beside the physical stability, the numerical stability especially for the time integration scheme is worthwhile to know. In the present work, the numerical stability is discussed in the structural level and the material level respectively.

Considering the structural system discretized by the finite element method, we have the governing ODE as follows

$$\begin{cases} \mathbf{Ma} + \mathbf{Cv} + \mathbf{f}^{\mathrm{int}} = \mathbf{f}^{\mathrm{ext}} \\ \mathbf{a} = \ddot{\mathbf{u}},\ \mathbf{v} = \dot{\mathbf{u}} \end{cases} \tag{84}$$

where $\mathbf{M}$ and $\mathbf{C}$ are the mass matrix and the damping matrix, respectively; $\mathbf{u}$, $\mathbf{v}$ and $\mathbf{a}$ are the displacement vector, the velocity vector and the acceleration vector, respectively; $\mathbf{f}^{\mathrm{int}}$ and $\mathbf{f}^{\mathrm{ext}}$ are the internal force vector and the external force vector, respectively.

To solve the ODE Eq. (84) in an explicit way, the central difference method is usually applied. We have the following scheme [3]

– First partial update of velocity

$$\mathbf{v}_{n+\frac{1}{2}} = \mathbf{v}_n + \frac{1}{2}(t_{n+1} - t_n)\mathbf{a}_n \tag{85}$$

– Update displacement

$$\mathbf{d}_{n+1} = \mathbf{d}_n + (t_{n+1} - t_n)\mathbf{v}_{n+\frac{1}{2}} \tag{86}$$

– Compute acceleration

$$\mathbf{a}_{n+1} = \mathbf{M}^{-1}\left(\mathbf{f}^{\mathrm{ext}}_{n+1} - \mathbf{f}^{\mathrm{int}}_{n+1} - \mathbf{C}\mathbf{v}_{n+\frac{1}{2}}\right) \tag{87}$$

– Second partial update of velocity

$$\mathbf{v}_{n+1} = \mathbf{v}_{n+\frac{1}{2}} + \frac{1}{2}(t_{n+1} - t_n)\mathbf{a}_{n+1} \tag{88}$$

The numerical stability in the structural level is governed by the following condition [3]

$$\Delta t = \alpha_{\mathrm{NL}}\Delta t_{\mathrm{crit}} \tag{89}$$

The critical time step Δt_{crit} could be expressed as

$$\Delta t_{\mathrm{crit}} = \frac{2}{\omega_{\max}} \le \min_e \frac{l_e}{c_e} \tag{90}$$

where $\omega_{\max}$ is the maximum natural frequency of the linearised system; l_e and c_e are the characteristic length and wave speed in element e. The phenomenological coefficient α_{NL} is introduced to account for the destabilizing effect of nonlinearities. The suggested values are $0.80 \le \alpha_{\mathrm{NL}} \le 0.98$. On the other hand, although the material damage, plasticity and rate dependency may yield slower wave speed than the linear elastic material, Belytschko et al [3] suggested that the critical time step evaluated by Eq. (90) should not be increased.

In the material level, the proposed numerical scheme in Sect. 5 could offer exact simulating results in the elastic loading stage and the unloading stage. Thus the pure nonlinear loading steps are considered in the discussion of numerical stability. For simplicity, we still consider the uniaxial tension. Recall Eq. (63), the plastic strain in the $k+1$ step reads

$$\epsilon^p_{k+1} = \epsilon^p_k + \theta^{p+}_k(\epsilon_{k+1} - \epsilon_k) \tag{91}$$

Perform Eq. (91) recursively and assume at the starting point $\epsilon_1 = \epsilon^p_1 = 0$, we have

$$\begin{aligned}\epsilon^p_{k+1} &= \sum_{i=1}^{k} \theta^{p+}_i(\epsilon_{i+1} - \epsilon_i) \\ &\le \theta^{p+}_k \sum_{i=1}^{k}(\epsilon_{i+1} - \epsilon_i) = \theta^{p+}_k \epsilon_{k+1}\end{aligned} \tag{92}$$

Expression Eq. (92) indicated that the numerically solved plastic strain is bounded. Thus the proposed scheme is unconditionally stable for the computation of plastic strain.

Then we should compute the $(\overline{\epsilon}^{e\pm}_r)_{k+1}$ based on Eq. (55). The stability of Eq. (55) is governed by the transformation matrix on the right hand side. By solving the eigenvalue equation of the transformation matrix in Eq. (55), we have the eigenvalues

$$\begin{cases}\lambda_1 = 1 \\ \lambda_2 = \frac{\gamma^{\pm}_a \beta^{\pm}_n}{(\alpha^{\pm}_n + \beta^{\pm}_n)(\gamma^{\pm}_a + \beta^{\pm}_n \Delta t_k)} \in (0,1)\end{cases} \tag{93}$$

Hence it is indicated that Eq. (55), with which $(\overline{\epsilon}^{e\pm}_r)_{k+1}$ could be numerically solved, is unconditionally stable.

The last step is to solve the stress by Eq. (66). For the simple uniaxial tension case, we have

$$\begin{aligned}\sigma_{k+1} &= (1 - d_{k+1}) E_0 \left(\epsilon_{k+1} - \epsilon^p_{k+1}\right) \\ &= \left\{1 - g^{\pm}\left[(r^{\pm}_d)_{k+1}\right]\right\} E_0 \left(\epsilon_{k+1} - \epsilon^p_{k+1}\right)\end{aligned} \tag{94}$$

It is observed that all the terms on the RHS of Eq. (94) are bounded. Thus we find that the proposed numerical scheme in material level is unconditional stable. All that we need is to pay attention to the numerical convergence which is governed by Eq. (69).

In the end, we reach the conclusion that the numerical stability is governed by the structural level. Thus during the numerical simulation, the critical time step is only confirmed by Eq. (89).

7 Numerical tests

To learn the performance of the proposed model, we perform a series of numerical tests under various of loading conditions. Except particular statement, the time step is chosen to be 10^{-6} s in the following numerical simulations.

Table 1 Model parameters for uniaxial tests

	Tension	Compression
Elasticity	E_0(35GPa), ν(0.18)	
Biaxial strength increase	N/A	$\frac{f_{bc}}{f_c}$(1.16)
Static random damage	λ^+(5.3)	λ^-(7.6)
	ζ^+(0.6)	ζ^-(0.6)
	ξ^+(20)	ξ^-(10)
Dynamic damage	γ^+_a(12)	γ^-_a(1.5)
	n^+(0.0002)	n^-(0.0005)
Plasticity	ξ^+_p(0.6)	ξ^-_p(0.4)
	n^+_p(0.1)	n^-_p(0.1)

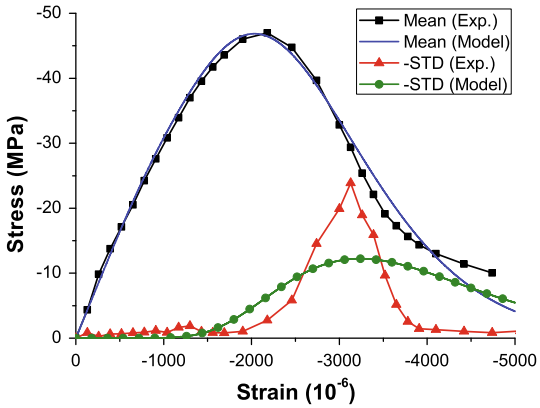

Fig. 5 Stress–strain curves under compression

7.1 Uniaxial tests

Numbers of model parameters (Table 1) are introduced in the proposed model to describe the properties of concrete. The bracketed values in Table 1 are chosen for the numerical simulations of uniaxial tests.

7.1.1 Monotonic static tests

Zeng et al. [50] carried out systematic experiments for the uniaxial and confined stress-strain performances of concrete. The mean values and the standard deviations (STD) of stress strain curves are characterized based on the testing data. On the other hand, the stochastic damage evolutions adopted in the present work yield the model results of the mean value and the standard deviations of stress strain curves. As shown in Fig. 5, the simulated mean value curve agrees well with the experimental results. The results of the standard deviation deserve further improvements, although they also show certain trends of the experimental results.

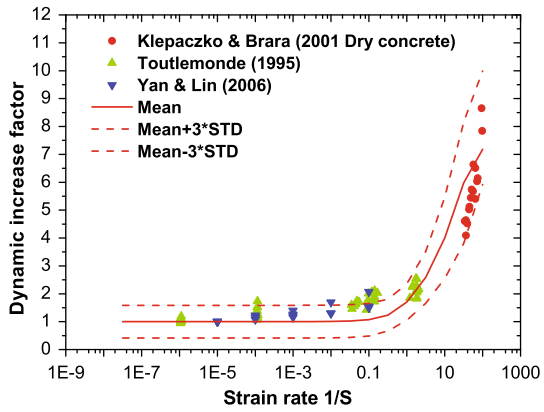

Fig. 6 Dynamic increase factor under tension

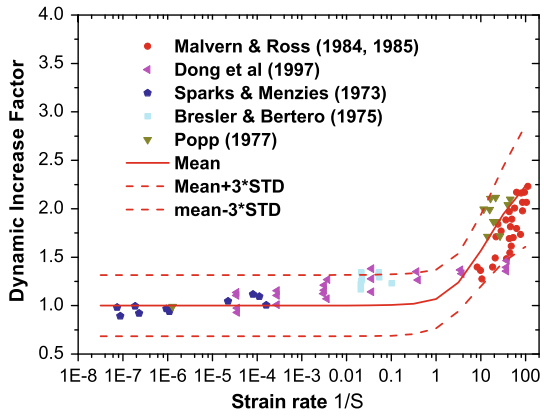

Fig. 7 Dynamic increase factor under compression

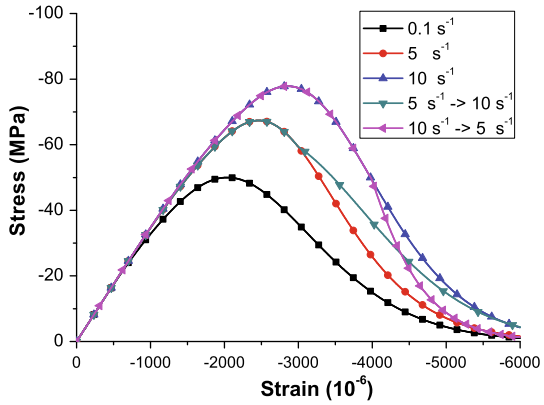

Fig. 8 Stress–strain curves subjected to different strain rates

7.1.2 Uniaxial dynamic behaviors

The numerical results of the dynamic increase factor, which is defined by the dynamic strength over static strength, are plotted in Figs. 6 and 7 against the collected existing experimental results [6,8,19,25,41,45,49]. The main trend of the increase of strength under fast loading is well reproduced.

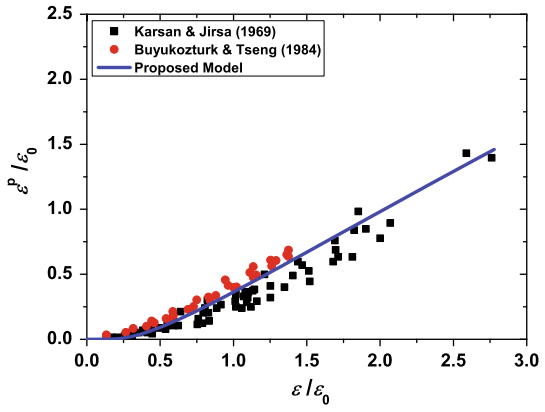

Fig. 9 Plastic strain of concrete under compression

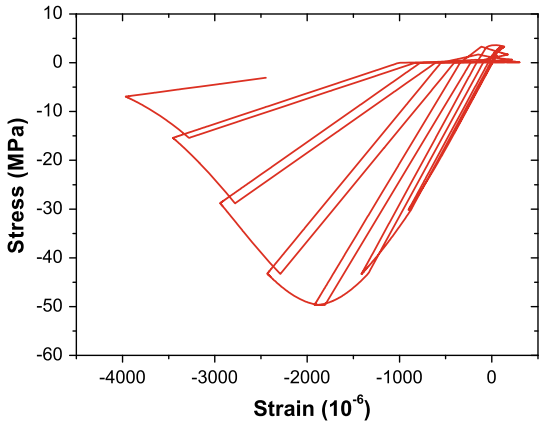

Fig. 10 Cyclic stress–strain curve under quasi-static loading

Meanwhile, the distributed domain of the testing data is also banded by the calculated Mean $\pm$ 3 $\times$ STD curves.

The stress–strain curves under different loading rates are shown in Fig. 8. The stress strengthening induced by the material rate-dependency is adequately reproduced. And the transitions of the stress–strain curves across different loading rates are smooth and convergent.

7.1.3 Cyclic tests

When subjected to the cyclic or the repeated loading, concrete often experiences residual strain, which is described by the proposed plastic model. The simulated results are plotted in Fig. 9 against the experimental data [7,18]. The total strain ϵ and the plastic strain ϵ^p are normalized by the peak strain ϵ_0 of the total stress–strain curve. And it is indicated that the model results agree well with the experiential data. The proposed plastic model works well in reproducing the residual strain of plain concrete.

The numerical tests for the concrete specimen under uniaxial cyclic loading are performed. The results are plotted in Figs. 10 and 11. The typical nonlinear behaviors of concrete,

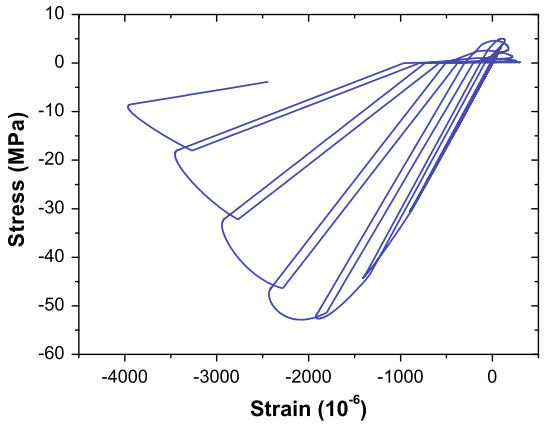

Fig. 11 Cyclic stress–strain curve under dynamic loading ($\dot{\epsilon} = 1.0\ s^{-1}$)

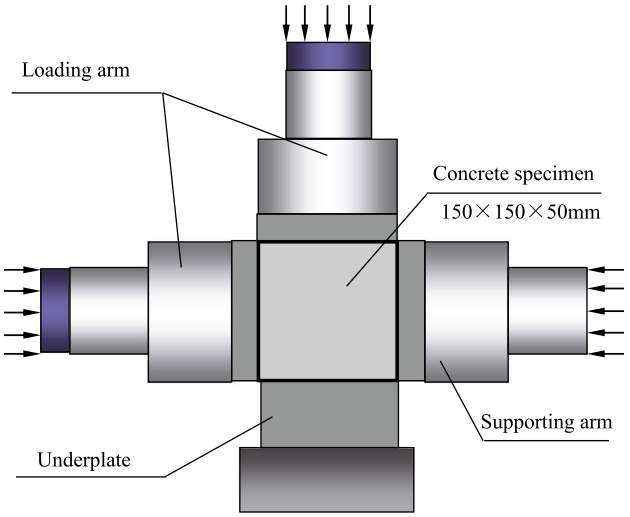

Fig. 12 Biaxial test set-up

Table 2 Model parameters for biaxial tests

	Tension	Compression
Elasticity	E_0(37.6GPa), ν(0.20)	
Biaxial strength increase	N/A	$\frac{f_{bc}}{f_c}$(1.30)
Static random damage	λ^+(4.92)	λ^-(7.70)
	ζ^+(0.30)	ζ^-(0.30)
Plasticity	ξ_p^+(0.6)	ξ_p^-(0.4)
	n_p^+(0.1)	n_p^-(0.1)

e.g. the strength softening, the residual strain, the degradation of stiffness, and the stiffness change between compression and tension, could be easily located on the simulated curves. And the hysteretic cycles could be also found, which dissipate energy throughout the unloading-reloading loops. The other interesting point is shown in the dynamic curve (see Fig. 11). We could find that the curve is smoothed at the

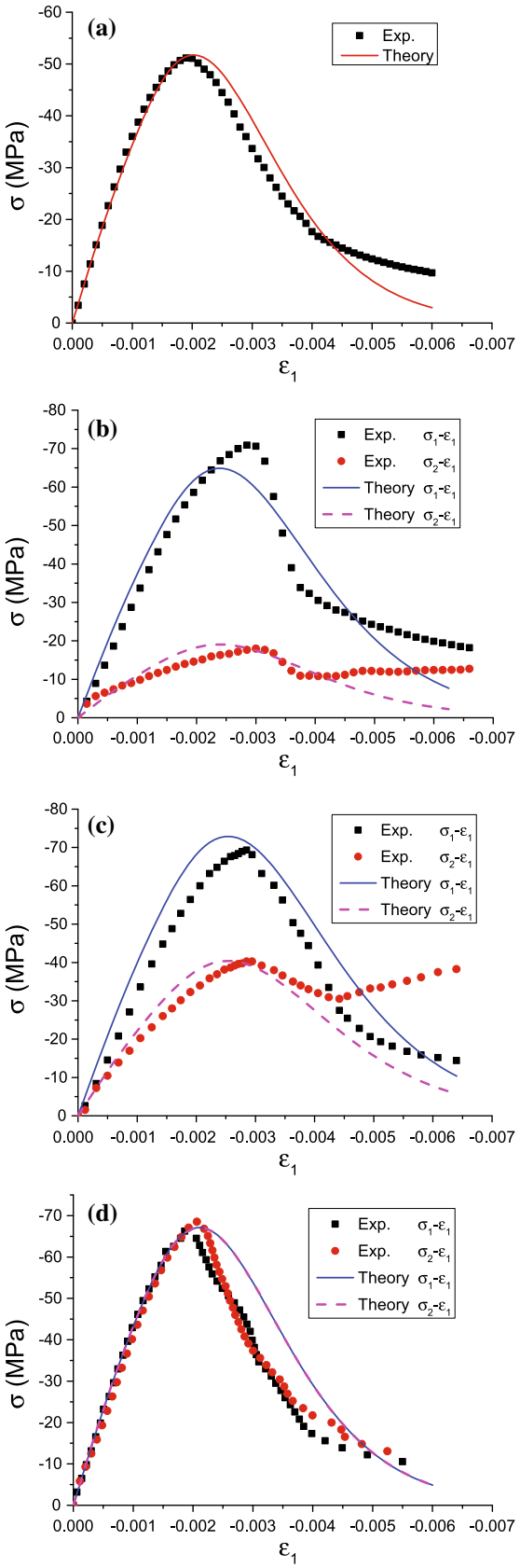

Fig. 13 Biaxial tests. **a** Uniaxial compression, **b** $\varepsilon_1 : \varepsilon_2 = 1.0 : 0.1$, **c** $\varepsilon_1 : \varepsilon_2 = 1.0 : 0.4$, **d** $\varepsilon_1 : \varepsilon_2 = 1.0 : 1.0$

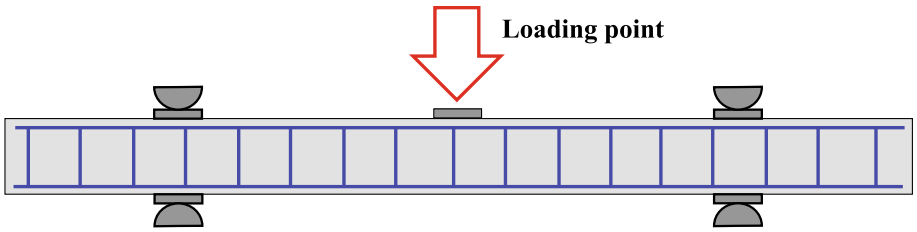

Fig. 14 Experimental set-up of RC beam

transition points linking the loading curve and the unloading curve by the rate-dependency.

7.2 Biaxial tests

The results of biaxial compressive experiments carried out by Ren and coworkers [33] are simulated to verify the multiaxial performance of the proposed model. The experimental set-up for the biaxial tests is shown in Fig. 12. The behaviors of high performance concrete specimens, with the dimension of $150 \times 150 \times 50$ mm, subjected to uniaxial and biaxial loading were experimentally investigated. The loads are applied by the top and left loading platens. And the strain rates were set to be less than 10^{-5} s^{-1} to simulate the static loading condition. To avoid the friction between concrete and steel platen, two slice of Teflon antifriction sheets are inserted into each contact surface. The uniaxial and biaxial compressive complete stress–strainstrain curves were obtained under strain control loading scheme. The tested stress is calculated by the applied force divided by the sectional area. And the tested strain the calculated by the relative displacement between correspond loading platens divided by the length of the specimen.

Due to the lack of reliable biaxial dynamic tests of concrete, only the static testing results are simulated in the present work. The bracketed values in Table 2 are chosen for the numerical simulations of biaxial tests. We assume the specimen is uniformed stressed because of the Teflon antifriction sheets. Thus only a single element is adopted to simulate the specimen. The simulated average stress–strain curves for the biaxial tests are shown in Fig. 13. The results in Fig. 13 are acceptably accurate up to the peak and in the first stage of the softening branch, but they diverge from the experimental curve in the late stage of the test. It suggests that the tail of the adopted average damage evolution functions in Eq. (35) may deserve further improvement.

7.3 Impact tests of RC beams

Saatci and Vecchio [36] performed experiments for the shear mechanisms of RC beams in University of Toronto Structural Laboratories. The experimental program consisted of two phases: static tests and impact tests. Thereafter, the experimental results were numerically simulated in the work of Ozbolt and Sharma [28]. The experimental set-up is shown in Fig. 14. The length of the beam is 4,880 mm, while the span is 3,000 mm. The overhangs were designed to amplify the inertia effect of the beam under impact loading. The upper supports were devised to prevent the uplift of the specimen. All specimens were doubly reinforced with two longitudinal reinforcing bars (nominal diameter=29.9 mm) on each side. And the closed stirrups (nominal diameter=7.01 mm) were used as transverse reinforcement. A 38 mm clear cover was provided between the beam surface and the steel bars.

Table 3 Simulated specimens

Specimen	Transverse reinforcement ratio (%)	loading pattern
SS0a	0	Static
SS0b	0	Impact
SS1a	0.1	Static
SS1b	0.1	Impact

Table 4 Model parameters

	Tension	Compression
Elasticity	E_0(35GPa), ν(0.20)	
Biaxial strength increase	N/A	$\frac{f_{bc}}{f_c}$(1.16)
Static random damage	λ^+(4.2)	λ^-(7.1)
	ζ^+(0.45)	ζ^-(0.6)
	ξ^+(20)	ξ^-(10)
Dynamic damage	γ_a^+(6)	γ_a^-(1.5)
	n^+(0.0002)	n^-(0.0005)
Plasticity	ξ_p^+(0.6)	ξ_p^-(0.4)
	n_p^+(0.1)	n_p^-(0.1)

Four beams (Table 3) of the experiments are simulated based on the proposed model. The bracketed values in Table 4 are chosen for the numerical simulations of RC beams. The drop-weight for the specimens SS0b and SS1b was 211 kg and the impact velocity is 8.0 m/s. Our numerical simulations are performed based on ABAQUS platform with our proposed damage model implemented by VUMAT.

The simulated damage contours, which actually indicate the crack patters of the beams, are shown in Fig. 15. The shear failure patterns could be clearly observed. The simu-

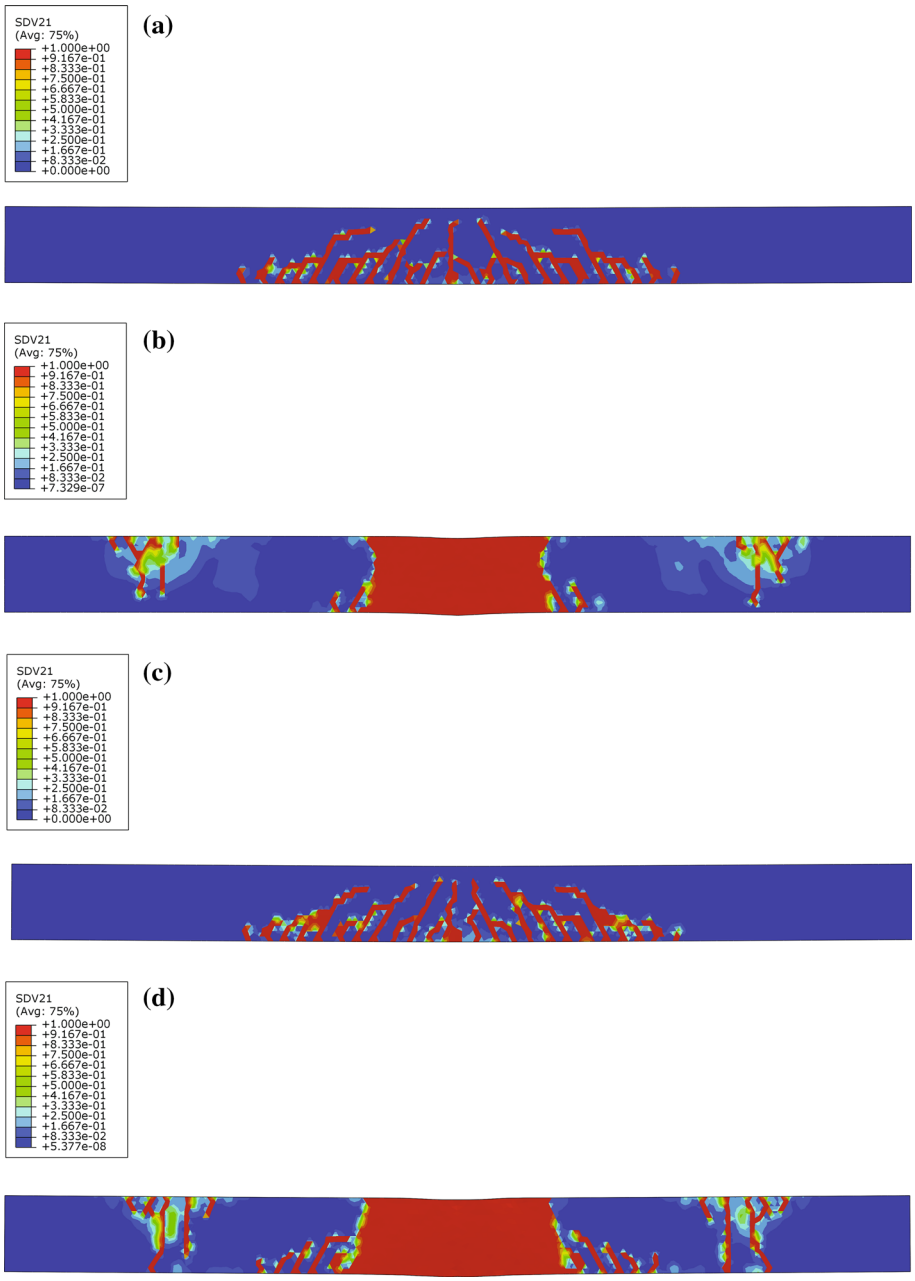

Fig. 15 Simulated contours of tensile damage D^+. **a** SS0a, **b** SS0b, **c** SS1a, **d** SS1b

Table 5 Simulated maximum reactions for the beams (KN)

Specimen	SS0a	SS0b	SS1a	SS1b
Experiment [36]	98	149	305	356
Ozbolt and Sharma [28]	112	158	346	372
Proposed model	101	145	267	313

lated maximum reactions of the beams are shown in Table 5. Agreements could be found among the experimental results of Saatci and Vecchio [36], the simulated results of Ozbolt and Sharma [28] and the simulated results of the proposed model.

8 Conclusions

Based on the theoretical developments and the numerical simulations in the present paper, numbers of conclusions could be given as follows:

– The typical nonlinear properties of concrete, including the strain softening, the residual strain, the unilateral effect and the hysteretic cycles, could be properly reproduced by the proposed model. Thus the structural nonlinear simulation performed based on the proposed model may capture the salient features of structural performance.

– By giving the scattering region of the testing data, the randomness of concrete is also reproduced by the proposed model. This aspect still deserve further investigations, which may develop the appropriate descriptions of the structural randomness and offer possible methods for the nonlinear structural reliability analysis.
– An explicit algorithm is developed for the numerical implementation of the proposed model in structural analysis. The algorithm tolerates excessive localization of strain and damage due to its robustness, but its global convergence requires particular attentions.
– The description of the material rate-dependency in the present work agrees well with experimental results. Moreover, a rather interesting point is detected. Although a linear differential system is proposed to develop the rate-dependent damage evolution, the nonlinear dynamic increase of material strength has been achieved due to the nonlinear coupling between the damage and the plasticity, which still deserves special attention in the upcoming study.
– Last but not the least, the rate-dependency not only enhances the material strength but also improves the material behaviors in a series of details. As shown by the numerical results, the transition points of the cyclic stress–strain curves are polished by the rate-dependency. Moreover, the increase of smoothness for the stress–strain curves may enhance the convergence of simulation and relieve the localization of deformation.

Acknowledgments Financial supports from the National Science Foundation of China are gratefully appreciated (GNs: 51261120374, 91315301 and 51208374). We would also like to express our sincere appreciations the anonymous referee for many valuable suggestions and corrections.

Appendix: Derivations of Stefan effect

In a viscous fluid, the stress σ_{ij} is often decomposed into the pressure p and the shear stress τ_{ij} as follows

$$\sigma_{ij} = \tau_{ij} - p\delta_{ij} \tag{95}$$

where δ_{ij} is the Kronecker delta. The constitutive law for the incompressible Newtonian fluid reads

$$\tau_{ij} = \mu(v_{i,j} + v_{j,i}) \tag{96}$$

where μ is the viscosity and v_i is the velocity in the i-th direction. And the incompressibility reads

$$v_{k,k} = 0 \tag{97}$$

The equilibrium without body forces and inertia effects reads

$$\sigma_{ij,j} = 0 \tag{98}$$

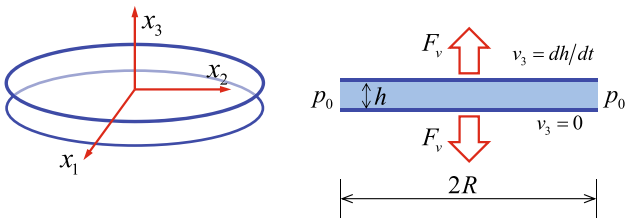

Fig. 16 Model problem of Stefan effect

Substituting Eq. (95) into Eq. (98) and using Eqs. (96) and (97), we have

$$\mu v_{i,jj} = p_{,i} \tag{99}$$

Combining Eqs. (97) and (99) and expanding the tensor expressions into regular expressions, we have the following governing equation for the incompressible Newtonian inertia free flow.

$$\begin{cases} \mu\left(\frac{\partial^2 v_1}{\partial x_1^2} + \frac{\partial^2 v_1}{\partial x_2^2} + \frac{\partial^2 v_1}{\partial x_3^2}\right) = \frac{\partial p}{\partial x_1} \\ \mu\left(\frac{\partial^2 v_2}{\partial x_1^2} + \frac{\partial^2 v_2}{\partial x_2^2} + \frac{\partial^2 v_2}{\partial x_3^2}\right) = \frac{\partial p}{\partial x_2} \\ \mu\left(\frac{\partial^2 v_3}{\partial x_1^2} + \frac{\partial^2 v_3}{\partial x_2^2} + \frac{\partial^2 v_3}{\partial x_3^2}\right) = \frac{\partial p}{\partial x_3} \\ \frac{\partial v_1}{\partial x_1} + \frac{\partial v_2}{\partial x_2} + \frac{\partial v_3}{\partial x_3} = 0 \end{cases} \tag{100}$$

The model problem to solve the Stefan effect is shown in Fig. 16. Two parallel, circular plates with radius R that are separated by a Newtonian (incompressible) liquid with viscosity μ and thickness h. The next step is to obtain the expression of the force F_v applied on the plates by solving Eqs. (100) with the boundary conditions shown in Fig. 16.

As the model problem is axisymmetric, Eqs. (100) could be casted into the following form.

$$\begin{cases} \mu\left(\frac{\partial^2 v_r}{\partial r^2} + \frac{1}{r}\frac{\partial v_r}{\partial r} + \frac{\partial^2 v_r}{\partial z^2} - \frac{v_r}{r^2}\right) = \frac{\partial p}{\partial r} \\ \mu\left(\frac{\partial^2 v_z}{\partial r^2} + \frac{1}{r}\frac{\partial v_z}{\partial r} + \frac{\partial^2 v_z}{\partial z^2}\right) = \frac{\partial p}{\partial z} \\ \frac{\partial v_r}{\partial r} + \frac{v_r}{r} + \frac{\partial v_z}{\partial z} = 0 \end{cases} \tag{101}$$

[34] further assumes

$$\begin{cases} \frac{\partial^2 v_1}{\partial x_1^2} \ll \frac{\partial^2 v_1}{\partial x_3^2}, \ \frac{\partial^2 v_1}{\partial x_2^2} \ll \frac{\partial^2 v_1}{\partial x_3^2} \\ \frac{\partial^2 v_2}{\partial x_1^2} \ll \frac{\partial^2 v_1}{\partial x_3^2}, \ \frac{\partial^2 v_2}{\partial x_2^2} \ll \frac{\partial^2 v_1}{\partial x_3^2} \\ \frac{\partial v_3}{\partial x_3} = 0, \ \frac{\partial p}{\partial x_3} = 0 \end{cases} \tag{102}$$

Subtstuting Eq. (102) into Eq. (101) yields

$$\begin{cases} \mu\frac{\partial^2 v_r}{\partial z^2} = \frac{dp}{dr} \\ \frac{\partial p}{\partial z} = 0 \\ \frac{\partial v_r}{\partial r} + \frac{v_r}{r} + \frac{dv_z}{dz} = 0 \end{cases} \tag{103}$$

The first equation in Eqs. (103) suggests the solution of v_r in the following form

$$v_r = \frac{z(z-h)}{2\mu}\frac{dp}{dr} \tag{104}$$

Substituting Eq. (104) into the third equation of Eqs. (103), we obtain

$$\frac{dv_z}{dz} = -\frac{z(z-h)}{2\mu}\left(\frac{d^2p}{dr^2} + \frac{1}{r}\frac{dp}{dr}\right) \tag{105}$$

An integration from 0 to h with respect to z gives

$$\frac{h^3}{12\mu}\left(\frac{d^2p}{dr^2} + \frac{1}{r}\frac{dp}{dr}\right) = v_z|_{z=h} = \dot{h} \tag{106}$$

The solution of Eq. (106) could be expressed as follows

$$p(r) = \frac{3\mu\dot{h}}{h^3}r^2 + C_1 \ln r + C_2 \tag{107}$$

Considering the conditions that $p(R) = p_0$ and $p(0)$ is bounded, we further have

$$p(r) = p_0 - \frac{3\mu\dot{h}}{h^3}(R^2 - r^2) \tag{108}$$

By integrating the additional pressure over the plate, we have the force induced by the viscosity

$$F_v = \int_0^R 2\pi r\big[p_0 - p(r)\big]dr = \frac{3\mu\pi R^4}{2h^3}\dot{h} \tag{109}$$

Considering the following expressions of stress and strain

$$\sigma_v = \frac{F_v}{\pi R^2},\ \dot{\epsilon} = \frac{\dot{h}}{h} \tag{110}$$

Eq. (109) further reads

$$\sigma_v = A\dot{\epsilon},\ A = \frac{\alpha_S\mu}{\gamma_h^2} \tag{111}$$

where the shape coefficient $\alpha_S = \frac{3}{2}$ and the aspect ratio $\gamma_h = \frac{h}{R}$ for circular plates. Although derived considering the circular plate, Eqs. (111) offers the general form of viscous coefficients A. And it is also observed that the aspect ratio γ_h plays a very important role for the rate-dependency between stress and strain rate besides the viscosity μ.

References

1. Abrams DA (1917) Effect of the rate of application of load on the compressive strength of concrete. ASTM J 17:364–377
2. Bazant ZP, Belytschko T (1985) Wave propagation in a strain-softening bar: exact solution. J Eng Mech 111(3):381–389. doi:10.1061/(ASCE)0733-9399(1985)111:3(381)
3. Belytschko T, Liu WK, Moran B (2000) Nonlinear finite elements for continuia and structures. John Wiley & Sons, LTD, New York
4. Bischoff PH, Perry SH (1991) Compressive behavior of concrete at high-strain rates. Mater Struct 24(144):425–450
5. de Borst R (2001) Some recent issues in computational failure mechanics. Int J Numer Methods Eng 52(1–2):63–95 5th US National Congress on Computational Mechanics, Univ Colorado, Boulder, Co. Aug 04–06, 1999
6. Bresler B, Bertero VV (1975) Influence of high strain rate and cyclic loading of unconfined and confined concrete in compression. In: the 2nd Canadian Conference on Earthquake Engineering, pp. 1–13. Hamilton, Ontario
7. Buyukozturk O, Tseng T (1984) Concrete in biaxial cyclic compression. J Struct Eng 110(3):461–476
8. Dong YL, Xie HP, Zhao P (1997) Experimental study and constitutive model on concrete under compression with different strain rate. J Hydraul Eng 7:72–77
9. Dube JF, Pijaudier-Cabot G, La Borderie C (1996) Rate dependent damage for concrete in dynamics. J Eng Mech ASCE 122(10):939–947
10. Duvaut G, Lions JL (1976) Inequalities in mechanics and physics. Springer-Verlag, Berlin
11. Faria R, Oliver J, Cervera M (1998) A strain-based plastic viscous-damage model for massive concrete structures. Int J Solids Struct 35(14):1533–1558
12. Freund LB (1973) Crack-propagation in an elastic solid subjected to general loading. 3. Stress wave loading. J Mech Phys Solids 21(2):47–61
13. Hatano T, Tsutsumi H (1960) Dynamic compressive deformation and failure of concrete under earthquake load. IBID pp. 1963–1978
14. Hsu TTC, Mo YL (2010) Unified theory of concrete structures. John Wiley, Singapore
15. Jason L, Huerta A, Pijaudier-Cabot G, Ghavamian S (2006) An elastic plastic damage formulation for concrete: application to elementary tests and comparison with an isotropic damage model. Comput Methods Appl Mech Eng 195(52):7077–7092. doi:10.1016/j.cma.2005.04.017
16. Ju JW (1989) On energy-based coupled elastoplastic damage theories: constitutive modeling and computational aspects. Int J Solids Struct 25(7):803–833
17. Kandarpa S, Kirkner DJ, Spencer BF (1996) Stochastic damage model for brittle materials subjected to monotonic loading. J Eng Mech ASCE 122(8):788–795
18. Karsan ID, Jirsa JO (1969) Behavior of concrete under compressive loadings. J Struct Div 95(12):2543–2563
19. Klepaczko J, Brara A (2001) An experimental method for dynamic tensile testing of concrete by spalling. Int J Impact Eng 25(4):387–409. doi:10.1016/S0734-743X(00)00050-6
20. Krajcinovic D, Fanella D (1986) A micromechanical damage model for concrete. Eng Fract Mech 25(5–6):585–596
21. Lee JH, Fenves G (1998) Plastic-damage model for cyclic loading of concrete structures. J Eng Mech ASCE 124(8):892–900
22. Lemaitre J (1971) Evaluation of dissipation and damage in metals submitted to dynamic loading. In: ICAM-1. Japan
23. Li J, Ren XD (2009) Stochastic damage model for concrete based on energy equivalent strain. Int J Solids Struct 46(11–12):2407–2419. doi:10.1016/j.ijsolstr.2009.01.024
24. Lorefice R, Etse G, Carol I (2008) Viscoplastic approach for rate-dependent failure analysis of concrete joints and interfaces. Int J Solids Struct 45(9):2686–2705. doi:10.1016/j.ijsolstr.2007.12.016
25. Malvar LJ, Ross CA (1998) Review of strain rate effects for concrete in tension. ACI Mater J 95(6):735–739
26. Needleman A (1988) Material rate dependence and mesh sensitivity in localization problems. Comput Methods Appl Mech Eng 67(1):69–85. doi:10.1016/0045-7825(88)90069-2
27. Niazi M, Wisselink H, Meinders T (2013) Viscoplastic regularization of local damage models: revisited. Comput Mech 51(2):203–216. doi:10.1007/s00466-012-0717-7
28. Ozbolt J, Sharma A (2011) Numerical simulation of reinforced concrete beams with different shear reinforcements under dynamic

impact loads. Int J Impact Eng 38(12):940–950. doi:10.1016/j.ijimpeng.2011.08.003
29. Peerlings R, deBorst R, Brekelmans W, deVree J, Spee I (1996) Some observations on localisation in non-local and gradient damage models. Eur J Mech A Solids 15(6):937–953
30. Perzyna P (1966) Fundamental problems in viscoplasticity. In: Advances in applied mechanics, Vol. 9. Academic Press Inc., New York, pp 243–377
31. Ren XD, Li J (2012) Dynamic fracture in irregularly structured systems. Phys Rev E 85: 055102. DOI:10.1103/PhysRevE.85.055102
32. Ren XD, Li J (2013) A unified dynamic model for concrete considering viscoplasticity and rate-dependent damage. Int J Damage Mech 22(4):530–555. doi:10.1177/1056789512455968
33. Ren XD, Yang WZ, Zhou Y, Li J (2008) Behavior of high-performance concrete under uniaxial and biaxial loading. ACI Mater J 105(6):548–557
34. Reynolds O (1886) On the theory of lubrication and its application to mr. beauchamp tower's experiments, including an experimental determination of the viscosity of olive oil. Philos Trans R Soc Lond 177:157–234. doi:10.1098/rstl.1886.0005
35. Ross CA, Tedesco JW, Kuennen ST (1995) Effects of strain-rate on concrete strength. ACI Mater J 92(1):37–47
36. Saatci S, Vecchio FJ (2009) Effects of shear mechanisms on impact behavior of reinforced concrete beams. ACI Struct J 106(1):78–86
37. Simo JC, Hughes T (1998) Computational inelasticity. Springer-Verlag, New York
38. Simo JC, Ju JW (1987) Strain-based and stress-based continuum damage models. 1. Formulation. Int J Solids Struct 23(7):821–840
39. Sloan S, Abbo A, Sheng D (2001) Refined explicit integration of elastoplastic models with automatic error control. Eng Comput 18(1–2):121–154. doi:10.1108/02644400110365842
40. Sloan SW (1987) Substepping schemes for the numerical integration of elastoplastic stress–strain relations. Int J Numer Methods Eng 24(5):893–911. doi:10.1002/nme.1620240505
41. Sparks PR, Menzies JB (1973) The effect of the rate of the loading upon the static fatigue strength of plain concrete in compression. Mag Concrete Res 25(83):73–80
42. Stefan MJ (1874) Versuche furdie scheinbare adhasion. In: Sitzungsberichte der Kaiserlichen Akademie der Wissenschaften Wiens, Mathematisch Naturwissenschaftliche Klasse, pp. 713–735
43. Takeda J, Tachikawa H (1971) Deformation and fracture of concrete subjected to dynamic load. In: the Int. Conference on Mech. Behavior of Materials, Concrete and Cement Paste, Glass and Ceramics, vol. 4. Kyoto, Japan, pp. 267–277
44. Tedesco JW, Ross CA (1998) Strain-rate-dependent constitutive equations for concrete. J Press Vessel Technol-Trans ASME 120(4):398–405
45. Toutlemonde F (1995) Impact resistance of concrete structures. Ph.D. thesis, Laboratory of Bridges and Roads (LCPC), Paris
46. Wang W, Sluys L, deBorst R (1997) Viscoplasticity for instabilities due to strain softening and strain-rate softening. Int J Numer Methods Eng 40(20):3839–3864
47. Wu JY, Li J, Faria R (2006) An energy release rate-based plastic-damage model for concrete. Int J Solids Struct 43(3–4):583–612. doi:10.1016/j.ijsolstr.2005.05.038
48. Xu XP, Needleman A (1994) Numerical simulations of fast crack-growth in brittle solids. J Mech Phys Solids 42(9):1397–1434
49. Yan DM, Lin G (2006) Dynamic properties of concrete in direct tension. Cement Concrete Res 36(7):1371–1378. doi:10.1016/j.cemconres.2006.03.003
50. Zeng SJ, Ren XD, Li J (2013) Hydrostatic behavior of concrete subjected to dynamic compression. J Struct Eng ASCE 139(9):1582–1592